



AALBORG UNIVERSITY
DENMARK

MATHIS BRETTE MORTENSEN

POLYMER SYNTHESIS FOR MORPHOLOGY CONTROL OF ORGANIC SOLAR CELLS

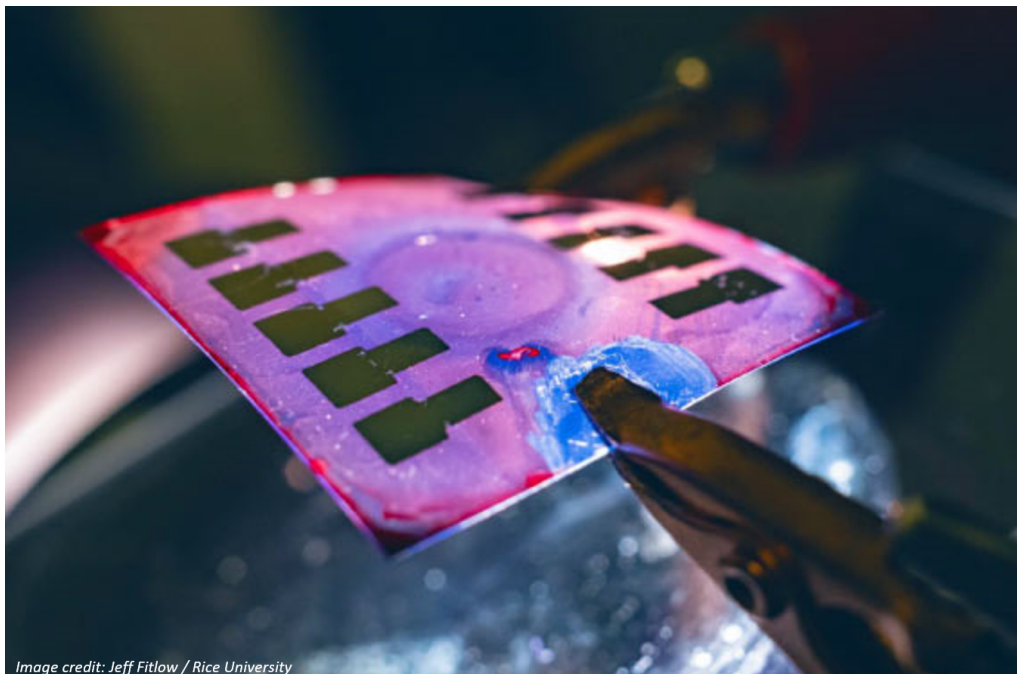


Image credit: Jeff Fitlow / Rice University



AALBORG UNIVERSITY
DENMARK

Department of Chemistry and Bioscience

Fredrik Bajers Vej 7H

DK-9220 Aalborg Ø

<http://en.bio.aau.dk>

Title:

Polymer Synthesis for Morphology Control of Organic Solar Cells

Theme:

Organic and Polymer Chemistry

Project Period:

Autumn 2021 to Spring 2022

Participant(s):

Mathis Brette Mortensen

Supervisor(s):

Donghong Yu

Page Numbers: 66

Date of Completion:

June 10, 2022

Abstract:

The technology behind organic solar cells (OSC) requires significant improvement to gather commercial interests for private companies to the same degree as silicon based solar cells. The unstable morphological nature of the active layer of OSCs is aimed to be improved by synthesizing both donor and acceptor semiconductor together as copolymers. Both vinyl and non-vinyl polymerization were attempted. The first synthetic step for monomer towards the vinyl copolymer has been performed thoroughly. For the non-vinyl polymerization, a well-known Suzuki cross-coupling reaction between a donor and an acceptor semiconductor was performed once, and twice under an emulsion polymerization in order to obtain donor-acceptor polymer particles in the nanometer range. In such size, these copolymers may be dispersed in water despite their hydrophobic nature which is of great interest for large-scale manufacturing.

Preface

This work is a one year Master thesis project from the Department of Chemistry and Bioscience at Aalborg University from September 2021 to June 2022. The theme of the Master thesis is organic and polymer chemistry with a strong focus on organic semiconductor synthesis. The experimental work is divided into two chapters. The first chapter thoroughly investigates the Diels-Alder cycloaddition of perylene and maleic anhydride as the first synthetic step towards vinyl polymerization. The second chapter involves the non-vinyl Suzuki cross-coupling polymerization of a donor and acceptor.

I would like to thank Donghong Yu associate professor for providing me theoretical and practical professional guidance in the field of organic and polymer chemistry, as well as offering me the opportunity to independently conduct my master thesis.

I would like to thank my parents Olivier and Jette, and my sister Emma for reading through my work as well as supporting me emotionally throughout the year. I would also like to thank Sonny and Miranda Skaaning for further reviewing and reading my thesis.

Aalborg University, June 10, 2022

Mathis Brette Mortensen
<mmorte20@student.aau.dk>

| Abbreviation | Description |
|---------------------|-------------------------------------|
| ATR | Attenuated total reflectance |
| BHJ | Bulk heterojunction |
| CB | Conduction band |
| DLS | Dynamic light scattering |
| DMF | Dimethylformamide |
| DP | Degree of polymerization |
| D/A | Donor and acceptor |
| EBE | Exciton binding energy |
| EDG | Electron donating group |
| E_g | Bandgap energy |
| E_{photon} | Photon energy |
| EtOAc | Ethyl acetate |
| EtOH | Ethanol |
| EWG | Electron withdrawing group |
| FT-IR | Fourier-transform infrared |
| GHG | Greenhouse gas |
| HOMO | Highest occupied molecular orbital |
| i-PrOH | Isopropanol |
| IQE | Internal quantum efficiency |
| LUMO | Lowest unoccupied molecular orbital |
| MeCN | Acetonitrile |
| MeOH | Methanol |
| NFA | Non-fullerene acceptor |
| NMR | Nuclear magnetic resonance |
| OSC | Organic solar cell |
| PCE | Power conversion efficiency |
| PDI | Polydispersity index |
| PHJ | Planar heterojunction |
| PP | Polypropylene |
| RCF | Relative centrifugal force |
| THF | Tetrahydrofuran |
| TLC | Thin-layer chromatography |
| TMS | Tetramethylsilane |
| UV | Ultraviolet |
| VB | Valence band |
| V_{oc} | Open circuit voltage |

Table of content

| | |
|--|-----------|
| Preface | 3 |
| 1 Introduction | 7 |
| 2 Problem Analysis | 9 |
| 3 Theory | 10 |
| 3.1 Solar Cells | 10 |
| 3.1.1 Historical Key Points | 10 |
| 3.1.2 State-of-the-art | 10 |
| 3.1.3 Basic Concept | 12 |
| 3.2 Active Layer | 13 |
| 3.2.1 P-N Junction | 13 |
| 3.2.2 Donor and Acceptor Interface | 14 |
| 3.2.3 Bulkheterojunction | 16 |
| 3.3 Synthesis | 17 |
| 3.3.1 Diels-Alder Reaction | 17 |
| 3.3.2 Suzuki Coupling | 18 |
| 3.3.3 Suzuki Coupling Emulsion Polymerization | 19 |
| 4 Vinyl Polymerization | 21 |
| 4.1 Perylene Anhydride Synthesis: Experimental Methods | 21 |
| 4.2 Perylene Anhydride Synthesis: Results and Discussion | 23 |
| 4.2.1 First TLC Overview | 23 |
| 4.2.2 Product Recovery Attempt | 25 |
| 4.2.3 Determination of the Appropriate Eluent System | 28 |
| 4.2.4 Additional Purification Steps | 35 |
| 5 Non-Vinyl Polymerization | 42 |
| 5.1 Suzuki Cross-Coupling: Experimental Methods | 42 |
| 5.1.1 Suzuki Cross-coupling Polymerization | 42 |
| 5.1.2 First Suzuki Cross-coupling Emulsion Polymerization | 45 |
| 5.1.3 Second Suzuki Cross-coupling Emulsion Polymerization | 47 |
| 5.2 Suzuki Cross-Coupling: Results and Discussion | 49 |
| 5.2.1 UV/Vis Spectroscopy | 50 |
| 5.2.2 Fluorescence Spectroscopy | 51 |
| 5.2.3 Dynamic Light Scattering | 53 |
| 5.2.4 Infrared Spectroscopy | 54 |
| 5.2.5 Nuclear Magnetic Resonance | 57 |
| 6 Conclusion | 62 |

| | |
|----------------------|-----------|
| 7 Perspective | 63 |
| Bibliography | 64 |

1 Introduction

During the official launch of the emission gap report (EGR) on October 26, 2021, the secretary-general of the United Nations, Antonio Guterres, stated that "with the present nationally determined contribution and other firm commitments of countries around the world, we are indeed on track for a catastrophic global temperature rise of around 2.7 °C [...] these announcements are essentially about 2050.". This statement does not align with the main goal outlined in the Paris Climate Accord (2015), which aimed to reduce the rise of global temperatures from 2 to 1.5 °C by 2050, compared to pre-industrial era temperatures. [1] Interestingly, according to the EGR of 2020 published by the United Nations Environment Program (UNEP), the long-term effect of the COVID-19 pandemic will only have slowed the global temperature rise by 0.01°C by the mid-century. In the short-term, however, the total overall carbon dioxide emissions from fossil fuels have dropped by 5.4 % compared to 2019 and the total greenhouse gas (GHG) emissions are also expected to drop similarly. Unfortunately, this does not alter the fact that a new all time high of GHG emissions was reached in 2019 at 59.1 GtCO₂ including land-use change. This rise has been constant for the past years with 55.3 GtCO₂ in 2018 and 53.5 GtCO₂ in 2017. [2–4]

All of these alarming facts are reminders of the current global environmental state that humanity has induced. Although turning a country entirely green is a political, social, and economical matter, ultimately, the issue lies behind the exploitation of fossil fuels as our main energy source, according to the EGRs. [2] The carbon dioxide release from fossil fuels accounted for 65 % of the total GHG emissions in 2019. Consequently, it is urgent to transition to a more renewable energy source. [2]

There are currently numerous green alternatives at humanity's disposal. The most popular and prevalent renewable energy sources include wind, solar, hydroelectric and geothermal energy. Depending on the condition and context of an area, wind turbines are more optimal than solar panels and vice versa. Solar cells, however, have significant improvement potential. Their power conversion efficiency (PCE) has increased each year since 1976. Research is being conducted into the various types of materials that pertain to the active ingredient or morphology of the transport layer. [5] One factor that contributes to the increased motivation behind the new developments into solar cell technologies is the nearly $1.5 \cdot 10^{18}$ kWh of solar energy that hits the Earth surface every year, which is more than 9700 times the annual global energy consumption of 2020. Along with its environmentally harmless dimension, it is only logical to optimize the harvesting potential of this great energy source. [6]

The field of research pertaining to solar cell systems splits into a large variety of groups: silicon, Ga/As, perovskite, CIGS, organic, quantum dots, amorphous hydrated silicon, and dye sensitized solar cells. While each category has its own research interest and developments, 95 % of the current commercialized solar cell market contains silicon cells. [7, 8] Though debatable, organic solar cells (OSC) are among the emergent fields that have

shown the most potential and gained the most amount of interest since the mid 90s. [5, 9] This is due to several positive qualities over traditional inorganic solar cells. By nature, OSCs can be easily manufactured in very large quantities as opposed to inorganic cells that often require high temperature and expensive vacuum systems. [10] OSCs are also flexible, lightweight, and transparent. Their flexibility and low weight even allow them to be rolled or printed onto surfaces with challenging curvatures such as windmill poles or the windows of a skyscraper. [7]

However, such advantages also come with disadvantages. Due to the physical and quantum limitations, as well as the lifetime and PCE of OSCs, traditional silicon solar cells are still preferred. The physical limitations that are currently being researched are: the decreased flow of electrons in organic semiconductors, the long term stability concerns and pairs of bound electron and hole easily recombined after photo-induced generation. [7]

Currently, the most popular organic solar systems used are a blend of donor and acceptor (D/A) molecules. As of april 2021, Ding et al. made an OSC with a PCE reaching 18.69 %. The material consisted of a ternary blend system of the donor D18-Cl with two acceptors, N3 and the fullerene PC61BM. [11] Here, they used a bulkheterojunction (BHJ) system, allowing for higher of interaction between the D/A surface area compared to planar junctions. Unfortunately, the chaotic distribution of the D/A interface of the BHJ systems prevents further improvement of organic photovoltaics (OPVs). [12] To tackle the issues concerning the electron transport, exciton recombination, and morphological instability of BHJ, a different approach is being researched, which involves block copolymerization to create a stronger connection in the D/A semiconductors. By covalently linking them, their morphology can better be controlled. In terms of performance, the PCE of block copolymers tends to fall behind those of BHJs. Therefore, this type of strategy can only be feasible for commercialization if the manufacturing process, manufacturing cost, solvent, PCE percentage, and every other parameter is. [12]

2 Problem Analysis

This project aimed to synthesize both vinyl and non-vinyl D/A copolymers to investigate the morphological control of the active layer materials via covalently binding the two semiconductors. For the vinyl polymerization, the aim was to synthesize a vinyl monomer with the structural moieties of donor and acceptor and follow-up polymerization. When planning the experiment, it included three chemical reactions for each semiconductor and one polymerization. Due to their triviality and time consumption, only the Diels-Alder cycloaddition of perylene and maleic anhydride has been investigated in details.

For the non-vinyl polymerization, the donor 2-[4-(1,3,2-dioxaborinan-2-yl)-2,5 -dihexyl phenyl] -1,3,2-dioxaborinane and the acceptor 4,7-dibromobenzo [c][1,2,5] thiadiazole were polymerized via the conventional Suzuki cross-coupling reaction. The particle size was controlled via emulsion polymerization. Two emulsions and one pilot polymerization were carried out. The chemical structure, optical properties, and particle size of the products were characterized via nuclear magnetic resonance (NMR), infrared (IR), ultraviolet and visible (UV/VIS) absorbance, fluorescence, and dynamic light scattering (DLS).

3 Theory

3.1 Solar Cells

3.1.1 Historical Key Points

In 1839, the French Physicist Aleandre-Edmon Becquerel discovered the first photovoltaic effect by illuminating platinum electrodes in acidic solution with sunlight and specific wavelength of light. [13] Nearly a century later, in 1946, the first modern solar cell using silicon was invented by Russel Ohl, an American engineer who also pioneered the area of the p-n junction. [14] In 1906, photoconductivity was first recorded for an organic material (anthracene) by the Italian scientist A. Pochettino. [15]

Two major breakthroughs in the history of OSCs were both made at the end of the 20th century. Firstly, Ching Wan Tang reached a PCE of 1 % with a full two-layer organic cell made with perylene pigment coupled with copper phtalocyanine. While already impressive at the time, considering that most OSCs were single-layered, the major breakthrough lied behind the design of the active layer. Ching Wan Tang followed the principle of D/A sensitized heterojunction, which became the foundation of nearly all emerging OPVs later on. While not exactly calling it D/A sensitization, he underlined the crucial importance of the interface between layers. Tang understood that this interface was the major component responsible for photoconductivity. [16]

The second breakthrough was the discovery of conductive polymers and BHJ solar cells. In 1974, Hideki Shirakawa, Alan Heeger, and Alan MacDiarmid synthesized and discovered the conductive property of polyacetylene. This discovery would award them the Nobel prize in 2000. [17] In 1991, Hiramoto et al. designed a three-layer OSCs consisting of two dye/dye layers of Me-PTC and H₂Pc with a mix of the two in between and reported a photocurrent two times higher than the version without the interlayer. [7] This set the ground for further investigation into using bulk mix of D/A. Four years later, Yu et al. made the first BHJ with a donor polymer and an acceptor molecule. By combining, poly(2-methoxy-5-(2'-ethyl-hexyloxy)-1,4-phenylene vinylene) or MEH-PPV with fullerene, they achieved a PCE of 2.9 %, significantly higher than the pure polymer. [9, 15] All these major breakthroughs would lead OSCs to become an emerging and new potential alternative energy source to fossil fuels.

3.1.2 State-of-the-art

The ever growing interest of OSCs has led to their rise as part of the third generation solar cells, along with quantum dots, dye sensitized, concentrated, perovskite, and nanocrystal solar cells. [17] The years following the major milestone were spent improving device fabrication and new D/A semiconductors with increased charge generation, dissociation and transport. Fullerene acceptors were prevalent until 2016 where an OSC using a non-

fullerene acceptor (NFA) yielded a new PCE record of 17 %. [7] The novel NFAs discovered by the same group [18], IDT-IC and IDTIDT-IC, are shown in Figure 3.1.

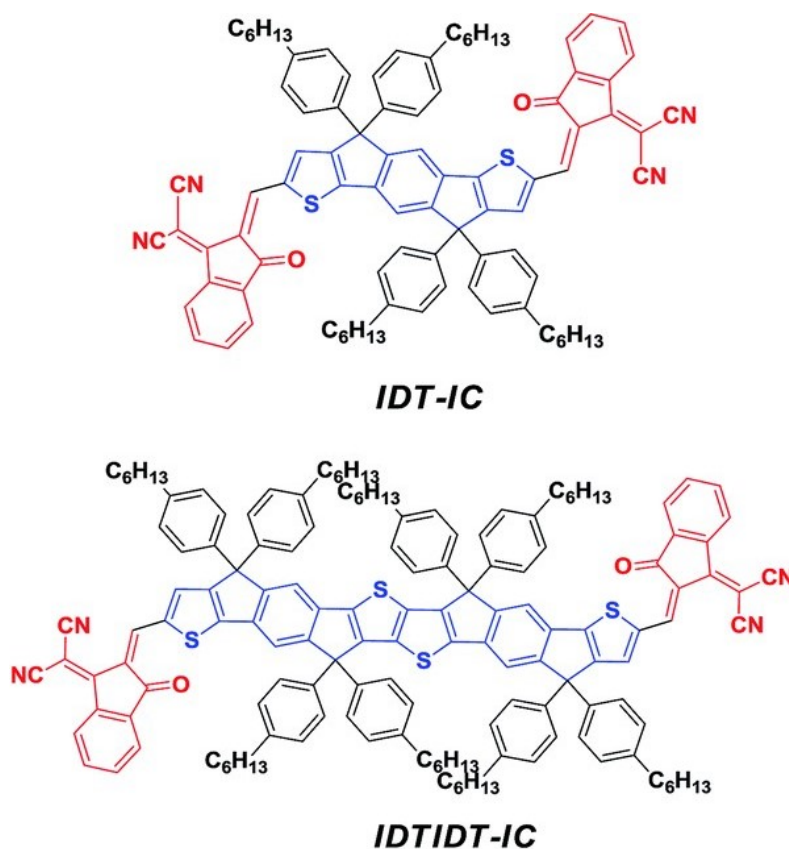


Figure 3.1. Chemical structures of the 10-heterocyclic rings indacenodithiophene (IDTIDT-IC) and the 5-heterocyclic rings indacenodithiophene (IDT-IC). The red moieties are 3-(dicyanomethylidene)indan-1-one groups with high electron withdrawing effect and good n-type transport properties. The blue moiety possesses an electron donating effect. Figure from [18].

Though they are still widely employed, fullerenes were limited by their innate weak absorption to light. Emerging low band-gap NFAs have light absorption spectrum matching the solar spectrum, and they provide higher short-circuit density and PCE than common fullerenes and derivatives. [19]

In recent years, donors such as PM6, PTQ10, D16, or W1 coupled with NFAs are the state-of-the-art single layer OSCs in term of performance. In particular, the focus for donor semiconductors is on fused-ring acceptor copolymers. [19]

In the mid-2021, the PCE record was held by Ding et al. [11] with a PCE value of 18.69 % from their work, certified 18.1 % from the National Institute of Metrology in Beijing. In here, they used a ternary system of one donor copolymer and two acceptors. The ratio of D:A₁:A₂ was 1:1.4:0.1 using D18-Cl:N3:PC₆₁BM as the active layer. The chemical structures of these compounds are shown in Figure 3.2. Note that a derivative of fullerene was used in this system for its electron mobility property. [11] As of the mid-2022, this current record is held by Zhu et al. [20] with a PCE of 19.6 % (certified 19.2 %) at

maximum value.

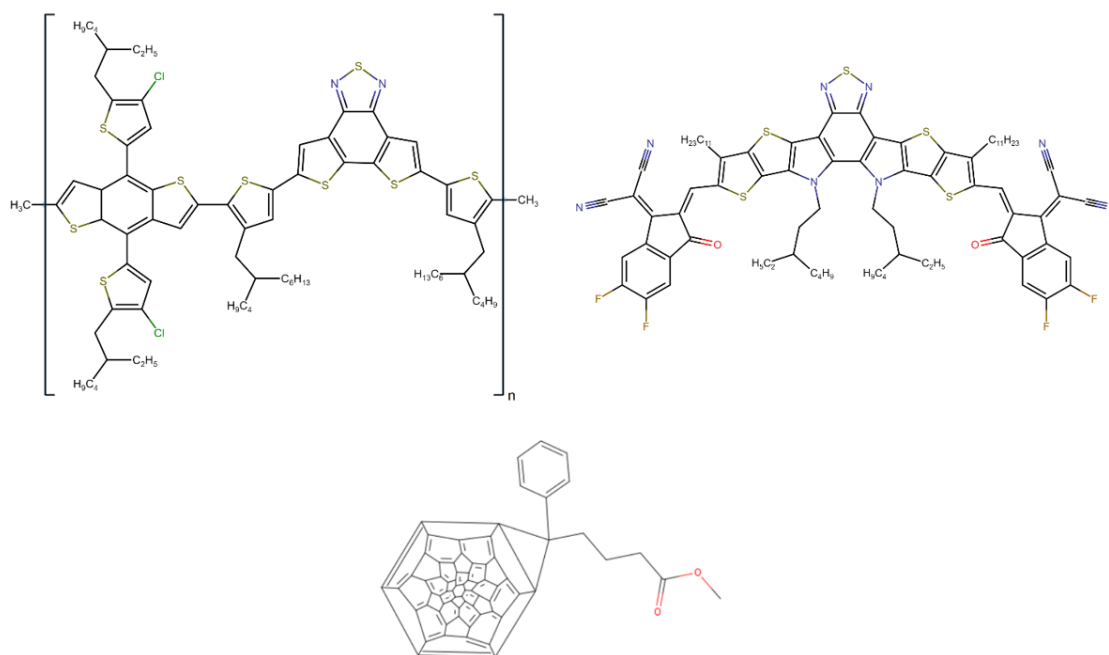


Figure 3.2. Chemical structures of D18-Cl on the top left, N3 on the top right, and PC₆₁BM on the bottom center. Structures drawn from sources available.

3.1.3 Basic Concept

A solar cell has many components. The general structure is shown in Figure 3.3 and includes a glass cover, a transparent adhesive, an anti-reflection coating, a p- and n-type layer of semiconductors and a front and back contact serving as electrodes. The glass cover offers protection against exterior damages such as small rocks or rain, the transparent adhesive lets light go through while adhering the layers together, and the anti-reflection coating prevents any photons from bouncing back out of the cell. The cell is then composed of its most important materials, the n- and p-type semiconductors, analogous to the D/A semiconductors mentioned earlier. They are responsible for the photo-active effects of the solar cells. A portion of sunlight is being absorbed in the active layer and incites the generation of free electrons. The most common cells are silicon ones where silicon is the only intrinsic material all throughout the active layer, and where the n- and p-type regions are doped with boron or phosphor. [21]

The photovoltaic effect of solar cells relies on three essential steps: 1. The absorption of photons into the p-n junction to generate pairs of electron and hole (or excitons for organic materials), 2. The separation of said charge carriers from each other, 3. Their collection at their respective electrodes creating an electrical potential difference. Optimizing each of these steps is the key to PCE improvement of solar cells. Their current understanding, and manufacturing is the resultant of nearly one and a half century of research. [17]

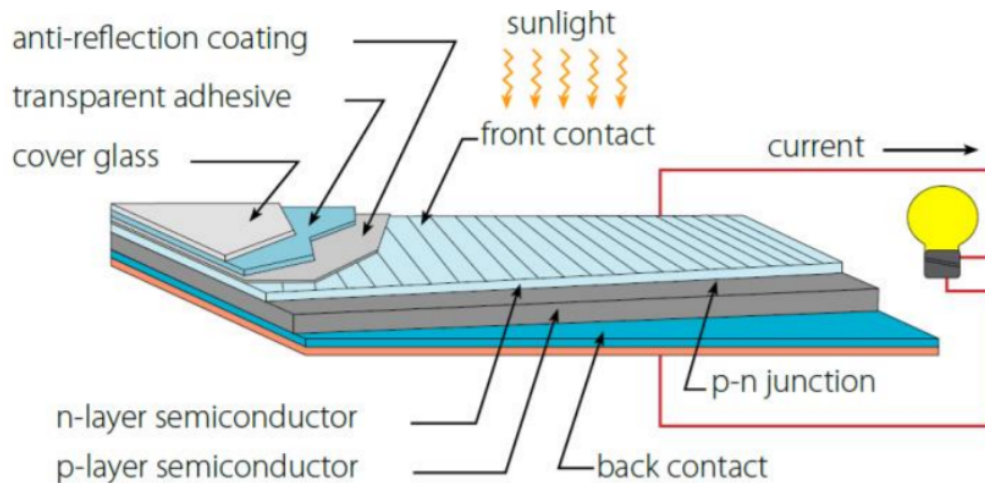


Figure 3.3. General structure of a solar cell including, a cover glass, a transparent adhesive, an anti-reflection coating, a front and back contact with the p-n junction in between. Figure from [21].

3.2 Active Layer

3.2.1 P-N Junction

The electrical current originating from any solar cells is generated via the interaction between a hole concentrated material and an electron concentrated material. These two materials are commonly referred to as p-type and n-type semiconductors. When combined into a single film or layer, they form a p-n junction. [22]

In most p-n junctions, an intrinsic semiconductor, such as silicon or gallium arsenide, is doped with impurities. For a p-type semiconductor, silicon is doped with an element presenting fewer valence electrons than silicon, such as boron. Similarly, a silicon based n-type semiconductor is doped with an element presenting more valence electrons than silicon, such as phosphorus. [23]

This difference in electron and hole concentrations within a single intrinsic material leads to a significant electron density contrast at the junction. In thermal equilibrium, this gradient causes the generated electrons, present in the n-type semiconductor, to diffuse through the p-type semiconductor in order to fill up the holes. Consequently, the holes from the p-type semiconductor are also diffusing to the n-type semiconductor creating a space charge or depletion region. [22] This phenomenon is depicted in Figure 3.4.

The exchange of charges at the p-n junction creates a negatively charged region in the p-type material and a positively charged region in the n-type material. Without any other external factors such as light or heat, this diffusion is not infinite and the length of the space charge region will remain constant. [22]

As electrons and holes flow through the material, the atom carriers are left charged, which induces an electric field from the positively charged region of the n-type semiconductor to the negatively charged region of the p-type semiconductor in the depletion region. The fact that the carriers are no longer neutral creates another gradient at the edges of the depletion

region inducing another diffusion force. In absence of any physical external factors, these factors balance themselves out and reach equilibrium. [22]

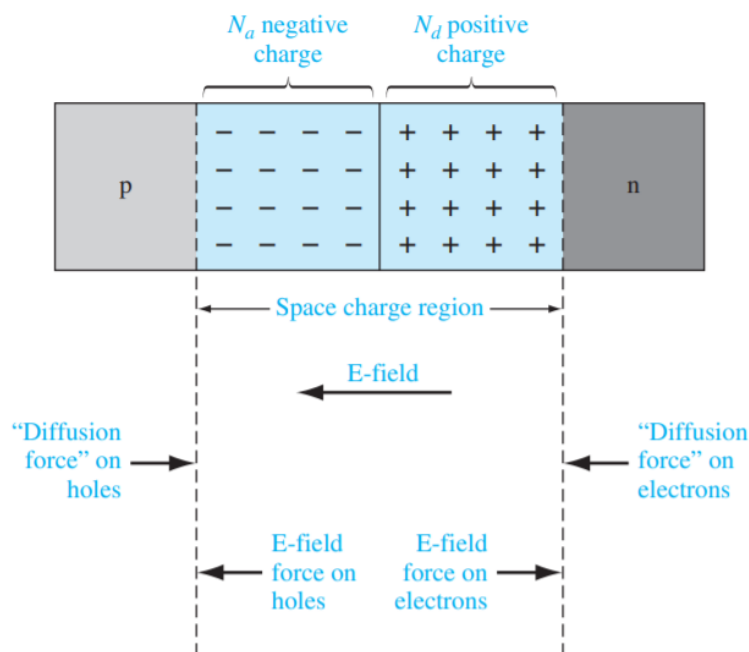


Figure 3.4. P-n junction with p-type and n-type regions, space charge region, electric fields, and diffusion forces. Figure from [22].

For a p-n junction to operate in a photosensitive manner, photons from sunlight must be absorbed. This is dependent on whether the photon energy (E_{photon}) is higher or lower than the bandgap energy (E_g) of the semiconductor. For the p-n junction to absorb photons, E_{photon} must be higher than E_g . When occurring, the valence electrons of a semiconductor will get excited and reach the conduction band, or the lowest unoccupied molecular orbital (LUMO). This excitation generate an electron-hole pair or exciton. The generation of excitons is the key factor for photo-generated electricity. When created, the electrons and holes dissociate to reach their respective electrode, thus producing an electrical current. Consequently, the active layer must match its absorption to the solar spectrum for maximum efficiency. [22]

3.2.2 Donor and Acceptor Interface

When referring to p-n junctions, inorganic systems are commonly thought of. For organic systems, however, this junction is labeled D/A interface. This is due to the fact that instead of than having an intrinsic organic semiconductor doped with electron and hole donating compounds, or homojunction, organic solar cells tend to prefer a heterojunction of two distinctly heterogeneous molecules. One harboring an electron donating property and the other an electron accepting property. [7] Note that while this is the majority of these systems, there still are some organic active layers that use homojunctions with diindenoperylene, rubrene, or anthracene as intrinsic materials for example. [7, 10, 24]

Unfortunately, organic molecules do not conduct electrons as readily as inorganic crystals

which is also illustrated by their different dielectric constant. The dielectric constant is unique to every material and is defined as the relative electric permeability (κ or ε_r) between the given material ε and the vacuum $\varepsilon_{(0)}$, as shown in Equation 3.1 below. [25]

$$\varepsilon_r = \frac{\varepsilon}{\varepsilon_{(0)}} \quad (3.1)$$

The dielectric constant is directly related to excitons and their attraction force, in other words, it defines the exciton strength of a material. The dissociation force of excitons has to overcome the attractive Coulomb force between them. Coulomb's law in the presence of a dielectric medium as shown in Equation 3.2 which illustrates the influence of a high or low dielectric constant. [7]

$$F = \left(\frac{1}{4\pi\varepsilon_r\varepsilon_0}\right)\left(\frac{q_1q_2}{r^2}\right) \quad (3.2)$$

Here, $\frac{1}{4\pi\varepsilon_0}$ is equivalent to the Coulomb constant ($K \approx 8.988 \cdot 10^9 N \cdot m^2 \cdot C^{-2}$) and q_1 and q_2 are the charges separated by the distance r . Following the Equation 3.1, $\varepsilon_0 \cdot \varepsilon_r$ is equivalent to the absolute permittivity ε of the material. The noteworthy element of this Coulomb equation is the fact that the absolute permittivity of the material is inversely proportional to the overall attractive force. The higher the dielectric constant, the weaker the Coulomb force between electrons and holes is. [7]

Organic semiconductors display very low dielectric constants where inorganic semiconductors display high ones, for example $\varepsilon = 4.4$ for fullerene and $\varepsilon = 11.9$ for silicon. This difference yields two different types of excitons: a hardly dissociative exciton called a Frenkel exciton for organic semiconductors, and an easily dissociating one called a Wannier-Mott exciton for inorganic semiconductors. This is in part explained by the overlapping orbitals of inorganic crystals, readily allowing the free carriers to diffuse through the medium. Organic molecules are disorganized, lacking a distinct pattern especially when tuned with electron withdrawing groups (EWG) and electron donating groups (EDG). [7] Frenkel excitons have the short lifetime of less than 1 nanosecond on average. Their strong Coulomb attractive force and limited lifetime lead to the main source of open circuit voltage (V_{oc}) loss in OSCs, exciton non-radiative recombination. [23]

The PCE is associated with V_{oc} , which in itself is the energy difference between the highest occupied molecular orbital (HOMO) of the donor and the LUMO of the acceptor, as portrayed in Figure 3.5 below. The challenge lies between balancing the V_{oc} and the energy required to excite the electron from the HOMO to the LUMO of the acceptor. The higher the LUMO of the acceptor, the higher the E_g . Hence, the E_{photon} must rise as such. [7]

To enable organic solar cells to generate and collect more excitons, novel concepts were invented to increase the D/A interface with the major discovery being the BHJ.

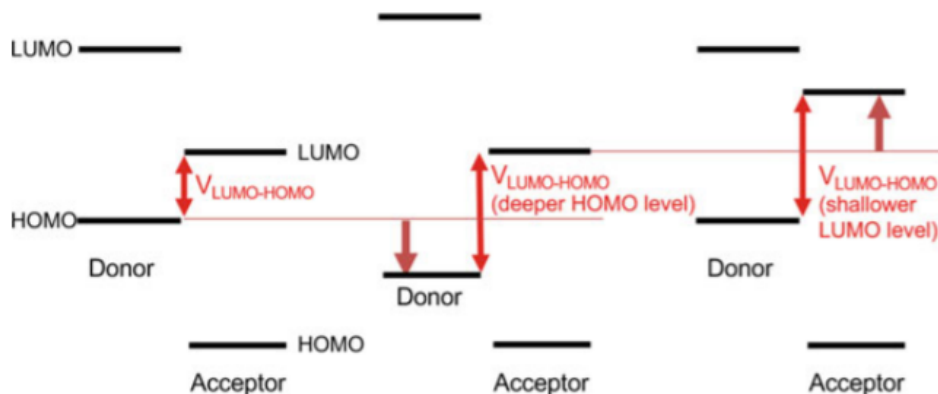


Figure 3.5. Different HOMO and LUMO levels of both donor and acceptor illustrating the change in $V_{LUMO-HOMO}$ or V_{oc} . Figure from [7].

3.2.3 Bulkheterojunction

A BHJ solar cell consists of a blend of D/A semiconductors as the active layer. This is in contrast to the planar heterojunction (PHJ) that has two distinct and separated layers. As mentioned earlier, this discovery serves as one of the most important breakthroughs in the research field of organic photovoltaic systems, as it allowed for a much larger amount of photogenerated free electrons and holes to be collected for further usage. [26] The two structures are shown in Figure 3.6.

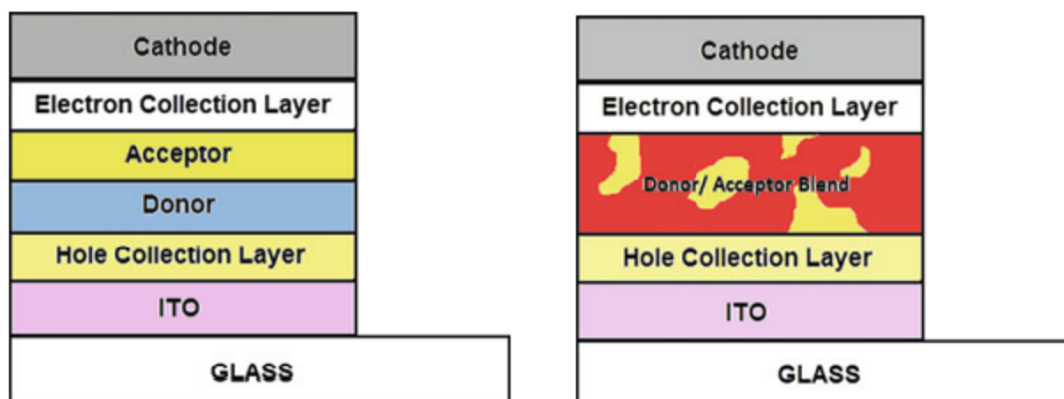


Figure 3.6. Schematic drawing of a donor and acceptor PHJ OSC and a BHJ OSC. These bilayers and blend make up the active layer, while the electron and hole collection layers make up the transport layer. Figure from [26].

The concept supporting this type of design is the exciton diffusion length in organic semiconductors. As opposed to the more classic inorganic semiconductors, the exciton diffusion length of organic semiconductors varies on average around 10 nm. This limitation heavily favors the non-radiative recombination of generated excitons in PHJ. By blending the two semiconductors relatively randomly, the surface area of interaction is significantly increased, allowing more exciton dissociation. [26] Nevertheless, the very strength of BHJ brings forth its limiting factor. As the blend allows more interface area, it also limits the charge transport pathway for the electrons and holes to reach their respective electrodes. This becomes the BHJ's most significant limiting factor. [10] Note that the mix of D/A

semiconductors is often seen as an intrinsic material with the p- and n- doped region analogous to concentration of D/A groups in the blend. Hence, it is not uncommon nor fundamentally wrong to refer to a D/A interface as a p-n junction. [7] For most cases, donors consist usually of polymers, oligomers, or conjugated pigments, and fullerene derivatives for acceptors. [23]

3.3 Synthesis

3.3.1 Diels-Alder Reaction

The Diels-Alder reaction, named after the two chemists who discovered its mechanism, is a stereospecific cycloaddition between a diene and a dienophile containing either a double or triple bond yielding a six membered ring. Overall, this reaction exchanges the two π -bonds from the reactants to two σ -bonds in the final product. The diene and dienophile can either have or be part of other functional groups other than alkyl or aryl groups. [27] The reaction equation is displayed in Figure 3.7 below.

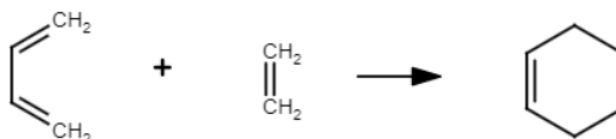


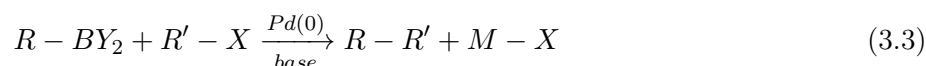
Figure 3.7. General chemical equation for a Diels-Alder reaction involving the cycloaddition of a compound containing a diene group and another one containing a dienophile group to yield an six-membered ring. Figure drawn from [28].

The Diels-Alder reaction mechanism is concerted, meaning that some bonds break while others form all in one step. The molecular state of the compound in formation is commonly referred to as the transition state. This transition state is highly thermodynamically unfavorable and thus quickly rearranges into the product's structure. [28]

The Diels-Alder reaction requires in most cases the use of heat to overcome an activation energy barrier depending on the energy contrasts of re-hybridization in the energy levels, the angle distortions, and the length alternations. Even for the processes that do not involve direct application of heat, the rate of reaction will increased when heat is applied. The essential criteria for this reaction to occur is the overlapping of molecular orbitals, which is dependent on the energy levels of the diene and dienophile which are influenced by the EDGs or EWGs present in either reactants. The presence of an EWG in the dienophile and an EDG in the diene enhances the reactivity of the Diels-Alder reaction. Another important criteria includes the essential s-cis conformation of the diene which allows both ends to point at the dienophile. If this conformation is hindered too much, the rate of reaction will lower or in worse cases become null. [27, 29]

3.3.2 Suzuki Coupling

In 2010, the Nobel prize in chemistry was granted to three organic chemists: Richard F. Heck, Ei-ichi Negishi, and Akira Suzuki for their work on palladium-catalyzed cross coupling reaction in organic synthesis. Thanks to their individual research, the very stable carbon-carbon sigma bond between molecules, chains, and other complexes can be formed through relatively simple steps, allowing for a wide variety of industrial and research applications. [30] The Suzuki cross coupling in particular is widely used in organic synthesis for its reactivity and safety. This coupling reaction involves an organohalide and organoboron group, a zerovalent palladium catalyst, and a base. The general reaction is shown in Equation 3.3 below.



Generally the boron groups are boronic acids $-B(OH)_2$, pinacol boronates $-B(OR_5O)$, boronic esters $-B(OR_1)(OR_2)$, or borane groups $-B(R_3)(R_4)$, as shown in Figure 3.8, a bromide or iodide for the halide, tetrakis(triphenylphosphine)palladium(0) or $Pd(PPh_3)_4$ for the catalyst and potassium or sodium carbonate for the base. [31]

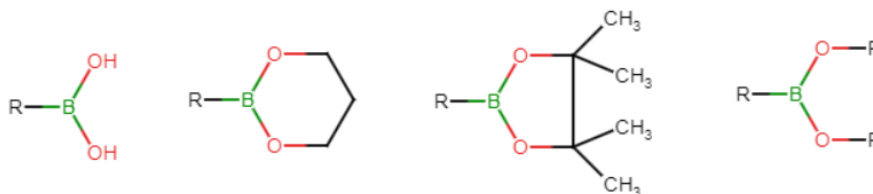


Figure 3.8. Chemical structure of several boron-based groups present as nucleophilic partners for typical Suzuki cross-coupling reactions.

The reaction cycle is shown in Figure 3.9. The mechanisms of the Suzuki cross-coupling reaction are split into three steps: oxidative addition, transmetalation, and reductive elimination. [30]

The first step involves the oxidative addition of a sp^3 C-halide electrophile and an R' group to the zerovalent palladium complex, which consequently increases the oxidation state of the palladium complex to +2. This step in itself has several sub-mechanisms. Depending on the reactivity of the halide and organic group, this reaction can be done through a concerted, S_N2 , radical, or ionic mechanism. Thereafter, the alkali earth metal from the base bonds with the halide forming a salt and then leaves the anion group of the base to form a bond with the catalyst. This anion group is subsequently substituted with the R group of the boronate species through the transmetalation step. The steric effect of the ligands helps induce the reductive elimination of the R and R' group from the palladium catalyst now reduced to its ground state. [32]

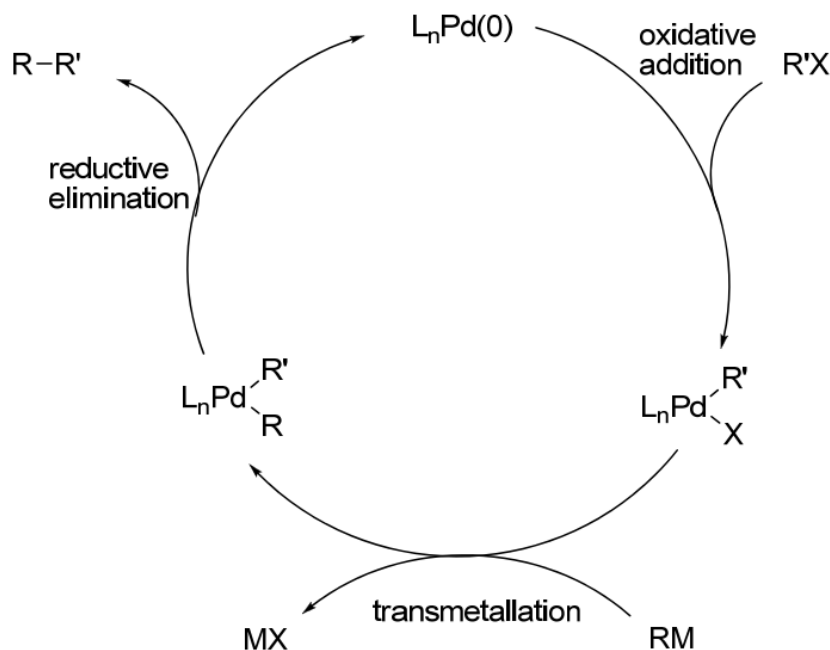


Figure 3.9. Catalytic cycle of palladium-catalyzed cross coupling reaction. The oxidative addition, transmetalation, and reductive elimination all occur during one Suzuki coupling reaction. [30]

3.3.3 Suzuki Coupling Emulsion Polymerization

A standard emulsion polymerization consists of two immiscible solvents, a surfactant, an initiator, if required, and monomers. Micelles can form with the help of the emulsifier and the two solvents, which then allows the polymer to grow inside the hydrophobic interior of the micelles. As water is often the continuous phase in such polymerization, the viscosity of the solution is relatively low, yielding excellent heat exchanges throughout the entire reaction. Emulsion polymerizations also have a higher rate of polymerization and molar mass when compared to other techniques. However, after the reaction, it is challenging to remove the presence of the emulsifier and the other polymer side-products. [33] In a Suzuki Emulsion polymerization, the cross coupling reaction is occurring inside the micelle as displayed in Figure 3.10.

The monomers and the palladium catalyst are dissolved in the organic solvent whereas the surfactant is dissolved in the aqueous basic solution. This combination allow for the advantages of an emulsion polymerization to apply for the suzuki coupling. [34] By alternating the different ratio of monomers, catalyst, solvent, and surfactant, the particle size can be controlled and remained at the nanoparticle range. [35] Moreover, the non-negligible low reaction temperature and use of water as a solvent is attractive for industrial applications. [34]

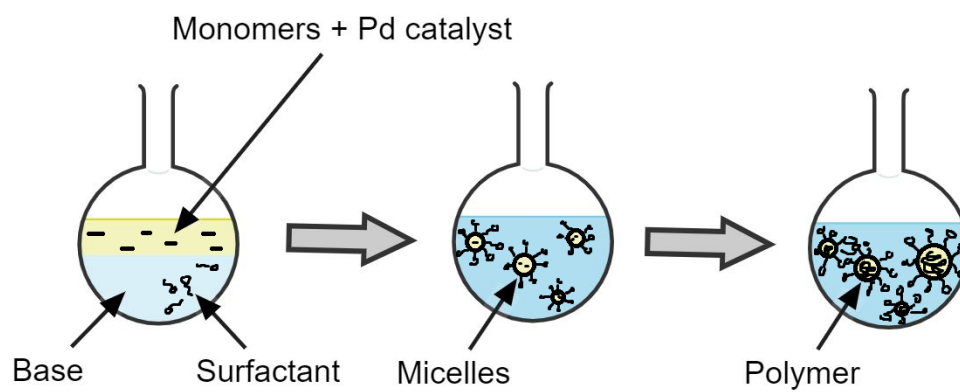


Figure 3.10. Suzuki cross coupling polymerization reaction in emulsion. The monomers are dissolved in the organic phase, then in the micelles after mixing, and polymerized when heated. Picture modified from [35].

4 Vinyl Polymerization

4.1 Perylene Anhydride Synthesis: Experimental Methods

The synthesis of the perylene derivative benzo(ghi)perylene-1,2-dicarboxylic anhydride was achieved by following the laboratory protocol of Alibert-Fouet et al. [36]. The chemical equation of the reaction is shown in Figure 4.1 below.

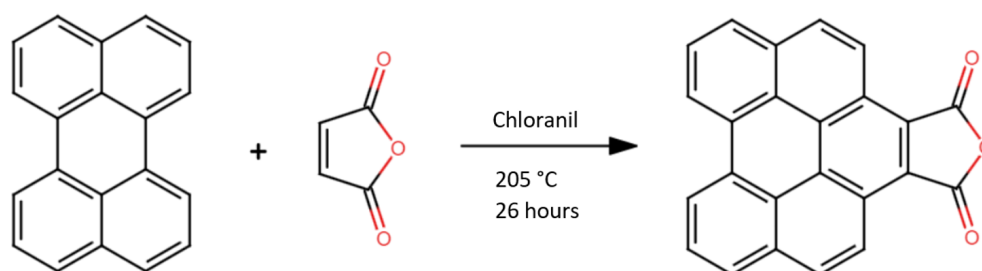


Figure 4.1. Chemical equation of the Diels-Alder cycloaddition of perylene and maleic anhydride into benzo(ghi)perylene-1,2-dicarboxylic anhydride. Reaction conditions from [36].

In a 500 mL three-headed round-bottom flask, 1.00 g ($3.95 \cdot 10^{-3}$ mol) of perylene (≥ 99 % Sigma-Aldrich[®]) is mixed with 2.07 g ($8.42 \cdot 10^{-3}$ mol) of tetrachloro-1,4-benzoquinone or chloranil, (99 % Aldrich Chemistry[®]) and 14.6 g ($1.49 \cdot 10^{-1}$ mol) of maleic anhydride (ICN Biomedicals, Inc.[®]) under reflux with anti-bump granules as stirring and control boiling on a hot plate. The two entries of the flask were plugged with rubber stoppers, one of them pierced with a temperature rod to monitor the temperature. The Alibert-Fouet protocol suggested the use of a silicon oil bath, however, a sand bath was preferred due to its safety and tidiness, regardless of how slow the heat transfer is. Even using aluminium foil to insulate the flask and sand as much as possible, it was only possible to reach a temperature of about 195 °C after 24 hours of reaction compared to 240 °C from the source. The flask was lifted then from the sand bath and a heating mantle was used instead. The flask heated relatively fast and a reflux ring was immediately noticed at the bottom of the condenser. In response, a second condenser was added. After around 20 min, the flask was already at 205 °C, but this temperature remained constant for 2 hours even at full power. The temperature difference was deemed negligible by increasing the reaction time from 10 minutes to 2 hours, as stated by Alibert-Fouet et al. [36] Pictures and drawings of the reaction setups using a sand bath and a heating mantle are shown in Figure 4.2 and Figure 4.3.

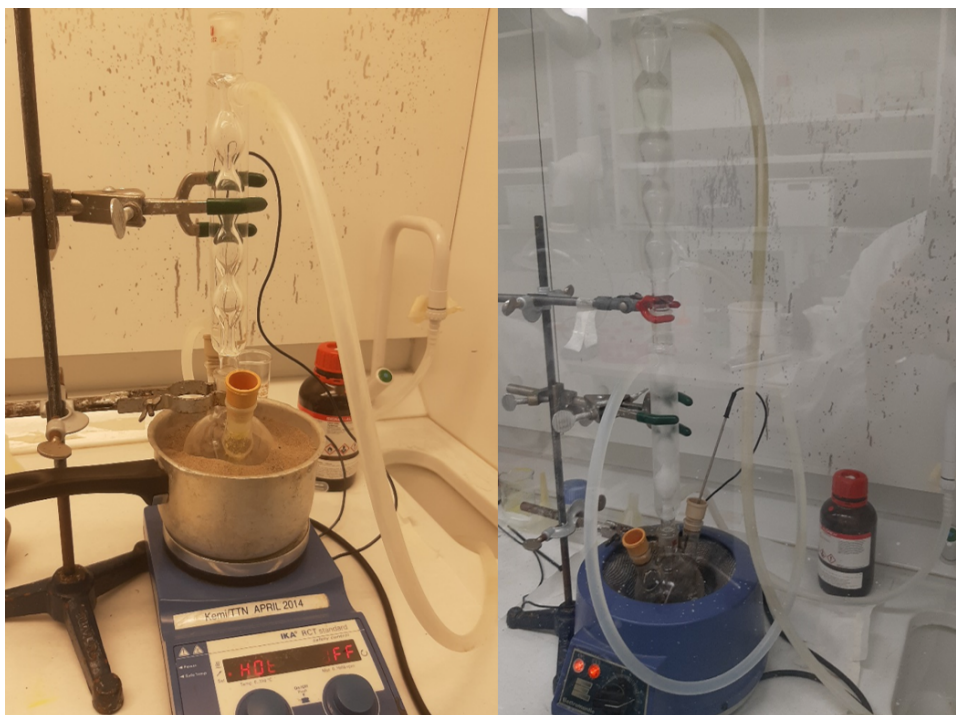


Figure 4.2. Pictures of the setup for the cycloaddition of perylene and maleic anhydride. The setup on the left uses a sand bath while the one on the right uses a heating mantle and two condensers.

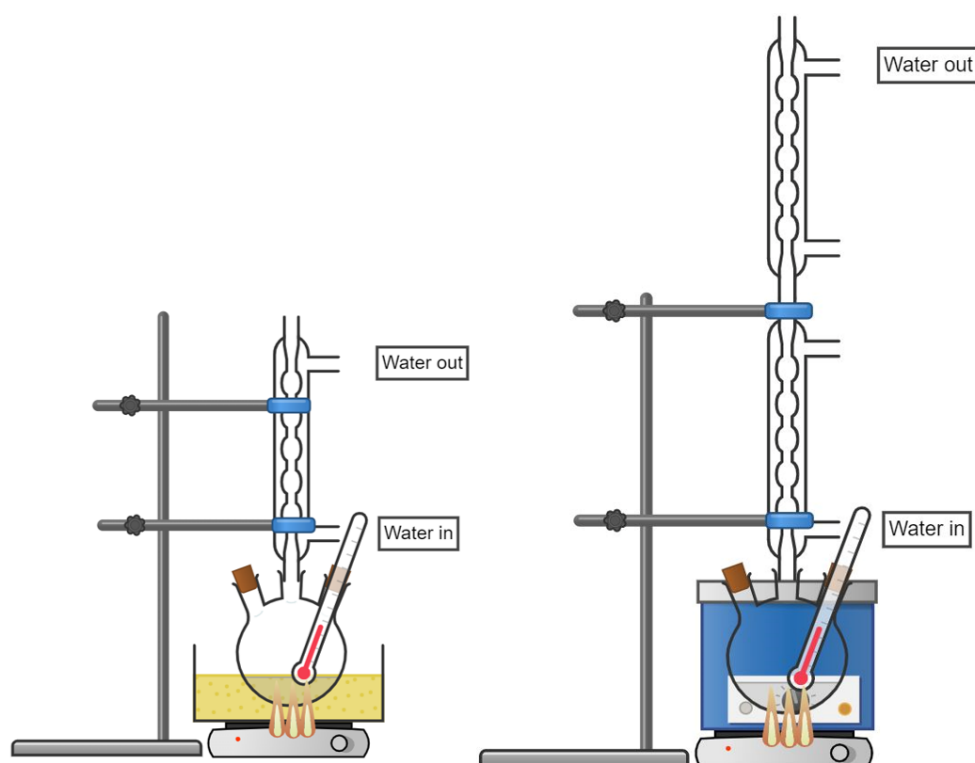


Figure 4.3. Schematic drawings of both setups to illustrate all components. Note that the two condensers are interconnected via a single tube from the top of the lower condenser to the bottom of the higher one.

The reaction was stopped and the flask was set to cool to about 100 °C. Upon reaching this temperature, the entire content of the flask solidified into a hard black mud. Some all isomer xylene was heated to about 35 °C and 100 mL of xylene was poured into the round-bottom flask. The resulting solution was hand shaken for about a minute and poured into an Erlenmeyer flask by using a funnel with a qualitative filter. The filtrate was kept and the residue was used further on. Note that the amount of the residue was very small and seemed stuck to the filter.

A solution of 200 mL ethyl acetate (EtOAc) and 100 mL chloroform was prepared in a beaker which was placed onto a hot plate set at to 100 °C. The content that was stuck onto the filter paper was transferred into the beaker by dropping some the EtOAc and chloroform solution onto the filter with a plastic pipette. The mixture became yellowish. The beaker was left to boil for about an hour. Simultaneously, another Erlenmeyer flask was prepared for hot filtration by placing it on a hot plate with another filter paper in a plastic funnel. When the hour had passed, the content of the beaker was poured into the Erlenmeyer flask and the content on the filter paper was collected. The overall separation and purification process is displayed in Figure 4.4.

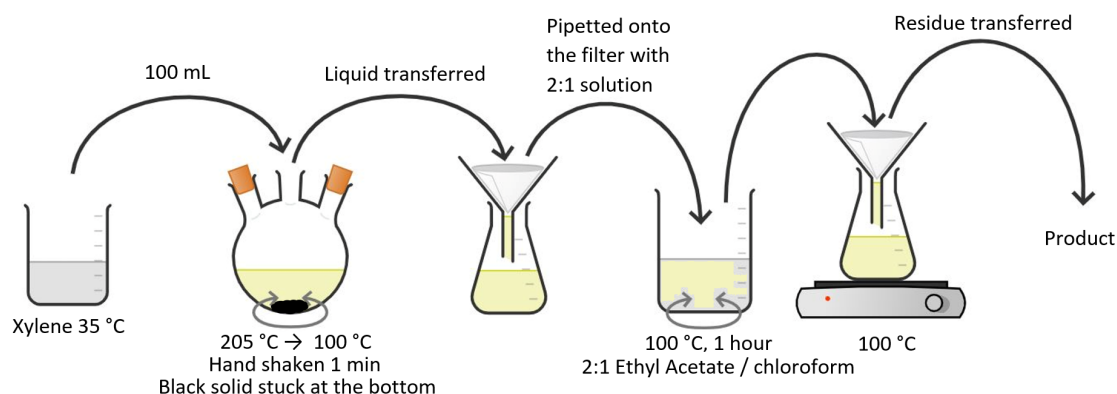


Figure 4.4. Separation and purification process first performed for the perylene anhydride product. Note that the black solid present in the round-bottom flask remained there even after pouring hot xylene and shaking for one minute.

The resulting residue from the hot filtration was completely absent. The lack of usable product led to conclude that the protocol has not been performed adequately and the product might still be either in the first Erlenmeyer flask with the first xylene solution, or with the initial round-bottom flask. Furthermore, a white solid had formed in the condenser during the reaction, which can be seen on the right picture from Figure 4.2. To identify the compounds, a thin layer chromatography (TLC) analysis was performed on every solution made from the reaction.

4.2 Perylene Anhydride Synthesis: Results and Discussion

4.2.1 First TLC Overview

A fraction of the yellow solution from the filtrate of the very first filtration was collected and labelled as "4" and the rest was concentrated through the rotary evaporator and

labelled as "5". The white crystals formed in the condenser was scraped and dissolved in chloroform (CHCl_3). This solution will be referred to as "6". All these compounds were also co-spotted with perylene (P), maleic anhydride (M), and chloranil (C) dissolved in CHCl_3 .

The eluent chosen for this TLC analysis was a 70/30 v% EtOAc/pentane. This was determined arbitrarily as the mix of the two solvents is a common eluent. As seen from Figure 4.5, the retention factor (R_f) is relatively high, with most of the compound eluting close to the solvent front, meaning that the mobile phase is possibly too polar. In other words, the ratio should be reduced to 50/50 v% if not less. It is relatively difficult to interpret exactly what is in 5 and 4 and simply impossible for 6 as no results were shown or found, though 5 does have a main spot very close to the one from perylene. Moreover, the dried sample of 5 shared the same color as perylene and could also be dissolved in CHCl_3 , leading one to believe that perylene is present in solution 5. The lack of the same comparison in 4 could be due to a too low concentration for the TLC to detect it.

For compound 6 on the other hand, the TLC plates alone were not sufficient enough to conclude anything. However, the substance barely dissolved in CHCl_3 and did readily in water, exactly as maleic anhydride. The condenser was, then, rinsed with water and almost everything came out after a couple of times. This somewhat proves that 6 is in fact recrystallized maleic anhydride. Now, the reason why it did crystallize in the condenser is most probably due to both a too low temperature in the flask and a too high water pressure in the condenser. The high water pressure allowed the condenser to always be at around 20 °C or less, whereas the melting point of maleic anhydride is at 50 °C, thus enough to recrystallize it. The loss of some maleic anhydride must have hindered the synthesis of the product. Another issue is the almost identical position of the perylene and chloranil compound on the TLC plates, further emphasizing the need to find a better eluent system.

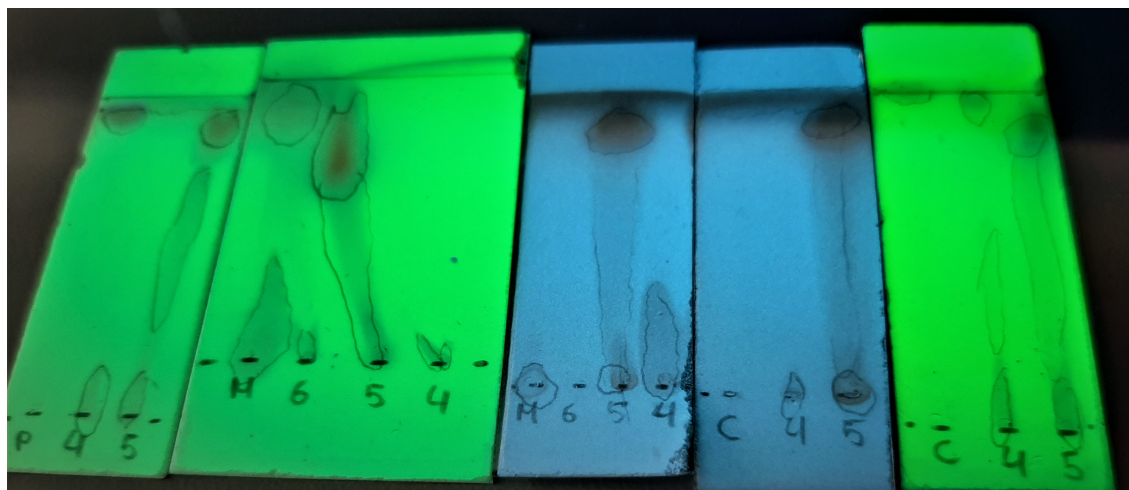


Figure 4.5. TLC of sample 4, 5, 6 co-spotted with perylene, maleic anhydride, and chloranil with a 70/30 v% EtOAc/pentane eluent system. The TLC analysis for chloranil and maleic anhydride were performed twice as they were not conducted properly the first time.

While the TLC plates do not conclude with certainty the presence of each reactant within the samples, they certainly demonstrate the presence of other compounds within these

samples. In fact, there is a chance that, as the separation and purification steps were performed wrongfully, the anhydride product remained in the very first round-bottom flask.

4.2.2 Product Recovery Attempt

The protocol for the separation and purification process has been performed once again with several modifications. The procedure is shown in Figure 4.6. A fraction of 95 °C all isomers xylene ($T_{bp} \approx 140^\circ\text{C}$) is poured into the round-bottom flask to extract any remaining products and non-polar side-products. The liquid-solid phase in the flask is hand shaken and the solution of xylene is filtered through gravity filtration into an Erlenmeyer flask until all 150 mL of hot xylene is used. The residue was washed with fresh xylene and transferred into another 500 mL round-bottom flask with 150 mL of 2:1 EtOAc/ CHCl_3 solvent. The mixture was boiled under reflux for 5 min at 60 °C with strong stirring. On the side, a ceramic funnel was pre-heated in an oven at 90 °C for hot filtration. Once the reflux was done, the content was quickly transferred into the hot ceramic funnel and the solution was vacuum filtrated. The filtrate was then left to recrystallize at -18 °C for 2.5 hours in a freezer. The sample was co-spotted with perylene on a TLC plate with the same eluent but no spots were visible. The solution was concentrated further and left to recrystallize several times with an even longer recrystallization period and resulted always in this outcome. The leftover solution was labelled "E".

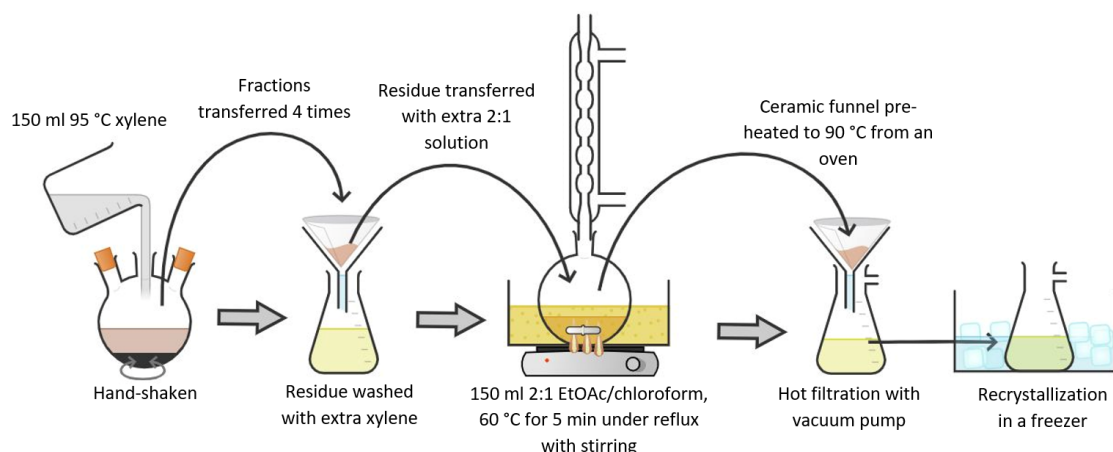


Figure 4.6. Scheme of the second attempt at the separation and purification of the perylene anhydride product. From then on, the final yellow solution is denoted "E".

This outcome could be explained by the fact that the xylene had not extracted the anhydride product from the flask. As it was believed, based on the protocol, that the perylene anhydride product is soluble in hot 2:1 EtOAc/ CHCl_3 , 150 mL of that solution heated to 55 °C was slowly poured several times into the round-bottom flask once again, and transferred this time into another beaker without filtration. The resulting solution looked much more red than the precedent sample and less see-through as well as containing some black dust at the bottom. This third product recovery attempt is schematically displayed through Figure 4.7.

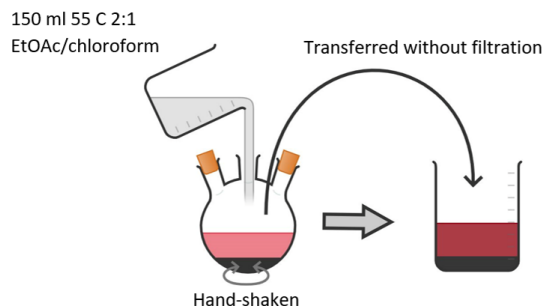


Figure 4.7. Scheme of the third attempt to harvest as much as the anhydride product as possible from the round-bottom flask. From then on, the red solution is denoted "F".

The red solution from the beaker is labelled "F". Compound 5, E, and F were co-spotted with perylene on three TLC plates with CHCl_3 and 1 v% acetone, pentane, and EtOAc as eluents. The first system was inspired by a published PhD work performing TLC on perylene based compounds [37] while the pentane and EtOAc were used for their relatively high polarity contrast. The plates are shown in Figure 4.8 below. Note that the denotation E has been inserted manually after taking the pictures. Initially, the sample was labelled "x2" as it was the product of running the separation protocol twice but it quickly became confusing as the experiment went on. Hence, for all TLC plates displayed further on, "x2" is interchanged to E.



Figure 4.8. TLC of sample 5, E, and F co-spotted with perylene dissolved in CHCl_3 with CHCl_3 and 10 v% acetone, pentane, and EtOAc as eluents.

Logically, the use of a very non-polar mobile phase such as pentane caused the compounds to interact more towards the stationary phase, thus remaining at the solvent front, and

inversely for the use of a polar eluent. On the left plate, E seems to show at least two spots, one at the baseline, like F, and one at the solvent front, like perylene. F also seems to have a second discreet spot with a R_f of around 0.75 dissimilar to sample E. When looking at the middle plate, not only does perylene display some level of fluorescence to which E nor F share, but it shows a R_f of around 0.4 as opposed to E, and F who does not even seem to elute at all away from the baseline. All in all, perylene does not seem to be present in either sample E or F according to the TLC plates. Though, both samples seem to contain some amount of impurities. These impurities include chloranil, polar side-products and non-polar side products. It was expected that F would contain several more concentrated spots as opposed to E as the latter was subjugated to more separation processes, but that does not seem to be the case. The eluent system or the relatively low concentration of F might be at cause.

To begin further purifying F, the black dust must be removed, as its insolubility in 2:1 EtOAc/ CHCl_3 was enough to conclude that this was not the perylene product. Consequently, hot filtration was performed twice on F but this black dust remained seen in the filtrate after filtration. This is the problem of using vacuum filtration on extremely small particles. To carry out a regular gravity filtration would probably solve the issue, but the slow process would most likely cool the funnel down with time. Using a Büchner funnel would probably be effective as it contains a porous filter already and can be pre-heated all while used afterwards for vacuum filtration. Another alternative would be to try celite, a powder originating from diatomaceous earth known for its small pores able to filter small particles that would readily pass through the filter. The black dust was, however, assumed to not alter the properties of the solution and was left as it was. On a side note, the red color of F after the hot filtrations looked like a concentrated version of the old orange from 5 from the very first purification process. So, as hot filtration was not performed correctly at all for the first separation procedure, it was applied to 5 with 150 mL of 2:1 EtOAc/ CHCl_3 . TLC was yet again performed on the newly hot filtrated samples and the plates are displayed in Figure 4.9. Firstly, a 1:1 ratio between EtOAc and pentane was tried with only 5 and the result shows a lot of long streaks and unclear spots. The same eluent as the left plate of Figure 4.8 was used instead.

The R_f of perylene is slightly more indicative of its absence in the other samples. It still looks like 5 is quite concentrated with at least 2 different compounds which both E and F seem to possess. A possibility to separate them would be to use liquid column chromatography. Unfortunately, the spots remain too close to both the solvent front and the baseline to separate the compounds efficiently. One must first find a suitable eluent system that will allow R_f to range from 0.2 to 0.8. Additionally, the perylene dissolved in CHCl_3 may have started to react and form other different compounds as two slight spots are noticeable at the bottom of the right plate. The other possibility would be that the solution was exposed to moisture and some impurities fell into the beaker.

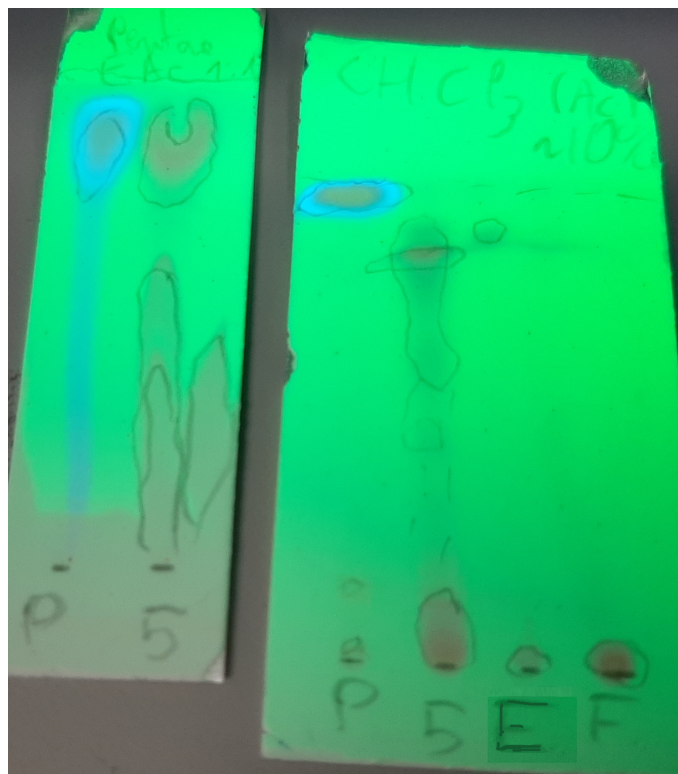


Figure 4.9. TLC of sample 5, E, F after hot filtration co-spotted with perylene with 9:1 CHCl_3 /acetone and 1:1 EtOAc/pentane as eluent.

4.2.3 Determination of the Appropriate Eluent System

Eluent systems are generally determined through literatures, however a TLC eluent system for the perylene anhydride specifically was not found. Thus, eluent systems for the reactants were thought to be a decent starting point. A 6:3:1 EtOAc/tetrahydrofuran (THF) /mEtOH (MeOH) and 3:2 acetonitrile (MeCN) / H_2O eluent systems were found for developing maleic anhydride and chloranil respectively on TLC plates.

All three samples share at least one compound non-polar enough to remain at the baseline. With that in mind, more polar eluents such as ethanol (EtOH), 2-propanol, and acetone were attempted. The TLC plates for the three eluent systems are shown in Figure 4.10. Acetone and 2-propanol gave unsuccessful results with big and long streaks at the bottom of the plates. While similar for EtOH, this eluent did rise the bottom compound from a $R_f = 0$ to $R_f = 0.25$ only for sample E, for some reason. To try and remove the long streaks still present, sample 5 and F were diluted by pipetting 1 mL of the stock solution to 37.5 mL of fresh 2:1 EtOAc/ CHCl_3 . It appears, when looking at both the 6:3:1 and 3:2 systems, that not only are they not successful eluent systems for these samples, but also they do not seem to elute maleic anhydride and chloranil well. The 3:2 system deserve a closer attention as the plate seem to have wrongfully been developed.



Figure 4.10. TLC of sample 5, E, and F co-spotted with maleic anhydride and chloranil. Three eluent systems were investigated: 6:3:1 EtOAc/THF/MeOH, 3:2 MeCN/H₂O, and EtOH. EtOH was tested twice with dilute sample of 5 and F.

For the 6:3:1 system, the spots are too close to both the baseline and the solvent front and therefore cannot be separated via column chromatography. The EtOH was interesting for E and maybe 5, but not for F. When looking at the second attempt with EtOH, sample 5 seemed too diluted, though it is possible to now see three spots for sample F. The 3:2 eluent system did not give clear spots and was attempted a second time. EtOH, 3:2 MeCN/H₂O, and a 1:1 EtOAc/CHCl₃ eluent systems were assessed and the resulting plates can be seen in Figure 4.11.

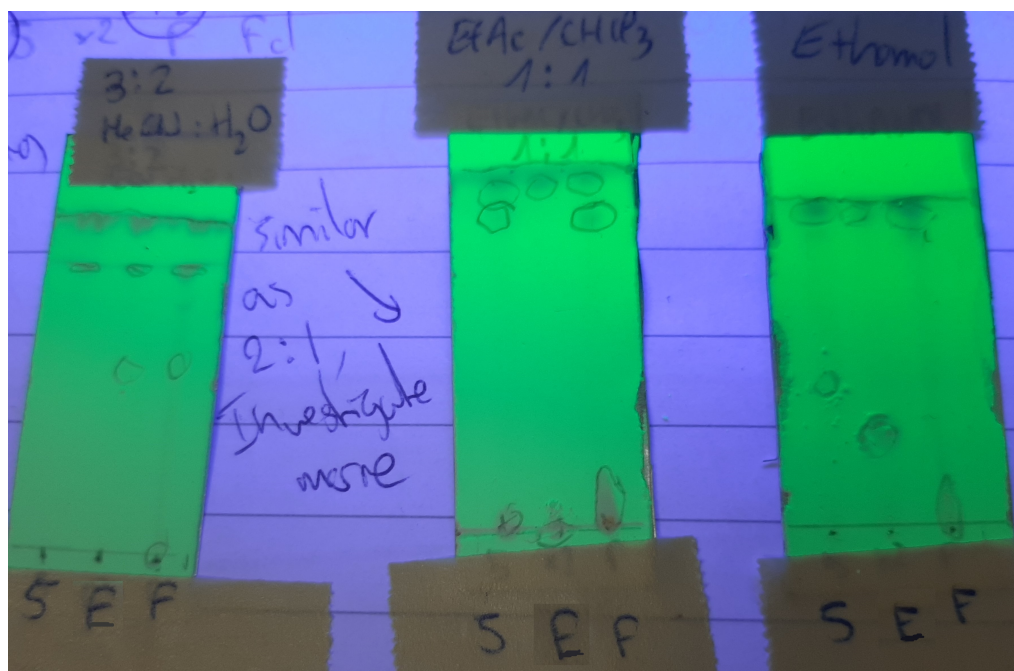


Figure 4.11. TLC of sample 5, E, and F with 3:2 MeCN/H₂O, 1:1 EtOAc/CHCl₃, and EtOH as eluents.

Until now, samples were loaded onto the TLC plates with 20 μL capillary micropipettes. By curiosity, the 5 μL ones were used instead and this caused the excessive blur and streaks to disappear from the plates, probably due to a much lower amount of sample loaded on the sheet. Hence, only 5 μL capillary micropipettes were used from then on.

On the first glance, the 3:2 eluent system provides some interesting spots with the two lines of three dots sitting side-by-side at the top of the plate. However, one can notice two solvent front lines when looking closely. What seems to have occurred is that the acetonitrile and water eluted separately with the top solvent front being water as it has its very distinct wave pattern that pure water has when used as eluent. Thus, while having different R_f , these two lines are most likely the same compound. The 1:1 ratio of EtOAc and CHCl_3 was intriguing as it did display two additional dots that are away from the solvent front and baseline of the sheet. The use of CHCl_3 in that eluent system was inspired by the traditional EtOAc and hexane/pentane eluent mixture, the fact that perylene is readily soluble in CHCl_3 , and the source using CHCl_3 and 1 v% [37] as the eluent for perylene based compounds mentioned in Section 4.2.2. The advantages of using mixture of solvents is that one can influence its polarity by simply increasing or decreasing the ratio of one of the solvents. In general for TLC, rising the polarity of the mobile phase causes the compounds to elute further towards the top of the sheet. This is obviously also influenced by the polarity of the compounds themselves, however, this effect is generally similar for all polarity. In other words, to lower the R_f of the compounds close to the solvent front, a more non-polar eluent should be used. That being said, as CHCl_3 is less polar than EtOAc, a 2:3, 1:3, 1:6, 1:9 EtOAc/ CHCl_3 ratio was tested. The results are shown in Figure 4.12. By curiosity, an eluent system of 10 v% acetone in CHCl_3 was tried additionally for comparison.

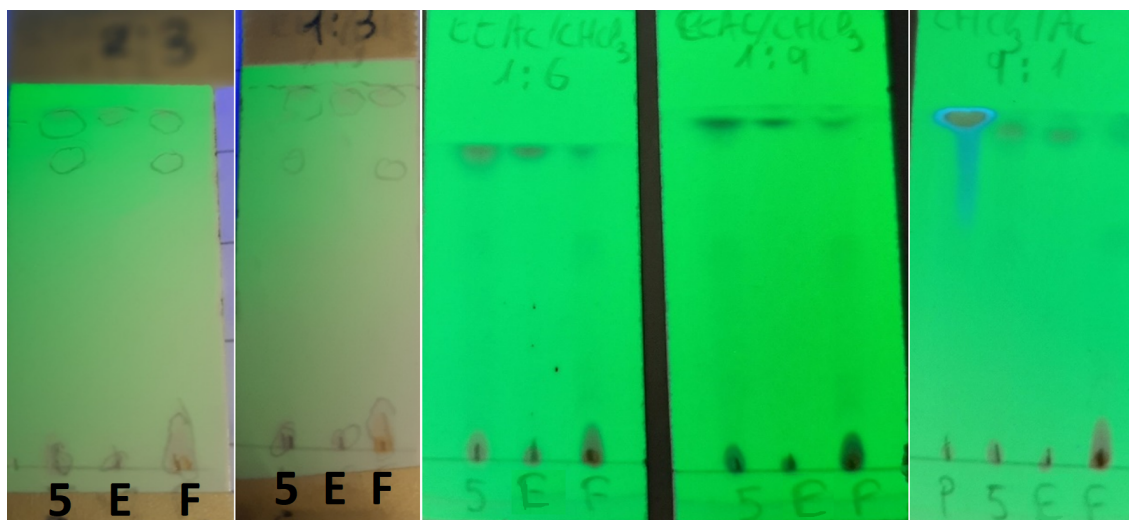


Figure 4.12. TLC of sample 5, E, and F with increasing ratio of CHCl_3 to EtOAc. The right-most plate has also perylene spotted and the eluent was 9:1 CHCl_3 /acetone. The two sheets on the right have much less opaque spots as their picture was taken 6 months after their development.

The higher fraction of CHCl_3 led to some of the slightly noticeable compounds to slowly lower their R_f from around 0.9 to 0.5 when starting at 2:3 to 1:9. Rising the ratio

further was not investigated as it did not seem to have the non-polar effect wanted for the compounds eluting at the very top of the sheet. One can notice that F has a slight spot right above the baseline, when looking at the 1:9 plate for instance. This is in accordance with the relatively impure nature of this sample, though this compound is in quite low concentration in comparison to the two major compounds at the baseline and solvent front.

For the second attempt at finding the optimal eluent ratio, a mixture of the polar solvent EtOAc and the non-polar solvent pentane was investigated. Figure 4.13 shows the influence of rising the ratio of pentane from 1:1 to 1:12. The opposite is seen in Figure 4.14 where EtOAc is increased from a 1:1 to a 6:1 ratio. Since pentane has the low boiling point of around 36.1 °C, the eluent preparation was done as quickly as possible to minimize evaporation of said solvent. EtOAc was also added first in the beaker, then followed by pentane.



Figure 4.13. TLC of sample 5, E, and F with increasing ratio of pentane to EtOAc.

As discussed earlier, the impact of rising the ratio of pentane to EtOAc made the compounds to elute closer to the baseline even though some compounds can be slightly seen at the top of the TLC sheet for the 1:12 ratio. These are most likely compounds possessing a very low polarity. Additionally, the compounds stuck to the bottom of the sheet make some relatively long streaks in the 1:1 to 1:3 ratios, while this is less and less noticeable for the rest of the systems. These streaks gave room for yet other non opaque spots slightly above them for the 1:9 and 1:12 ratio systems. These spots are only present for sample 5 and F. Similarly, a compound can be seen eluting in the middle of the TLC plate for the 1:9 and 1:12 ratio. This is correlation with the fact that sample E was purified in a much more efficient way, thus the presence and absence of certain compounds from sample E in comparison to 5 and F logical. While this system gave some insight on the content of the three samples, the R_f of the compounds from all said samples are yet to elute away from the solvent front and baseline for efficient separation through liquid chromatography. Hence, increasing the ratio of EtOAc was also investigated.

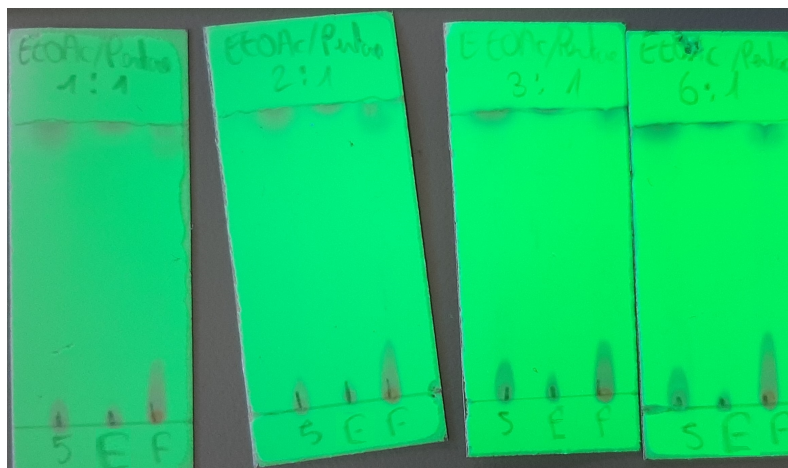


Figure 4.14. TLC of sample 5, E, and F with increasing ratio of EtOAc to pentane.

The polarity of EtOAc in regard to the compounds was expected to allow them to elute further from the baseline, as this solvent is also commonly used in TLC. That was shown not to be the case when raising from a 1:1 to a 6:1 EtOAc to pentane ratio. Higher ratios were not adapted, as the results seem to remain constant throughout the four plates. The streaks from the baseline do appear to slightly extend as the polarity of the mobile phase rises. An eluent system including pentane, EtOAc, and CHCl_3 together was thus considered to not be suitable for such samples.

Other empirical eluents were searched to hopefully yield the targeted R_f . While working on this search, another group from our department happened to be working with the chemical modification of cyclodextrins and used a peculiar eluent system consisting of a 5:3:1:1 ratio of isopropanol (i-PrOH), H_2O , ammonia (NH_3), and EtOAc. Out of curiosity, this eluent was tried on both the reactants and the samples. The resulting TLC sheets are shown in Figure 4.15 down below.

Initially, this mixture was speculated to exhibit a too high degree of polarity for the compounds, causing them to elute mostly at the solvent front. However, the eluent system not only separated the compounds of all samples relatively well, but also yielded excellent R_f . The possibility for the failure of earlier eluent attempts likely occurred due to EtOAc lacking strong polarity. It is now possible to examine the different compounds individually.

Sample 5, E, and F display two, three, and four distinct spots respectively. All three samples possess a compound eluting at the solvent front which, when looking at the right TLC plate, could be corresponding to chloranil. While the mobile phase is highly polar, the non-polarity of chloranil prevents it from any intermolecular interaction with the stationary phase, that is, the hydroxide groups of the silica sheet. However, the chloranil co-spot does depict a slight streak under the solvent front, thus it is not impossible for chloranil to be absent of the three samples. Starting from the top of the sheet, the next dot with a R_f of around 0.70 displays a compound of slight concentration in sample E, and F but not in 5. Yet again, this R_f , as well as the one underneath, may match the one of maleic anhydride. The fact that these two compounds are relatively close to each other makes it hard to associate maleic anhydride with any of them. The low solvent front reduces the precision

in R_f . A direct so-spot of maleic anhydride and sample F was performed much later and can be seen in Figure 4.16. This analysis was performed some time afterwards, which caused some of the least polar solvent of the eluent to evaporate, leaving H_2O and $i\text{-PrOH}$ to raise the spots higher on the plate. Here it is possible to see the direct correlation of maleic anhydride with the middle compound of sample F.



Figure 4.15. TLC of sample 5, E, F along with the perylene, chloranil, and maleic anhydride reactants. The eluent used was a 5:3:1:1 mixture of $i\text{-PrOH}$, H_2O , NH_3 , and $EtOAc$

Back to Figure 4.14, the dot for maleic anhydride at $R_f = 0.5$ is present for all three samples. Sample F has a definitely higher concentration of that compound than the two other samples and that is confirmed by the highly simplified nature of the purification procedure performed to yield F. Lastly, a compound remains at the baseline for sample F only. One could speculate that this is also the case for perylene, however, perylene displays fluorescence, while this is not shown for any of the samples. Hence, as this compound elutes at the baseline, its polarity has to be higher than maleic anhydride which may very well be maleic acid.

The previously attempted eluent systems, while being unsuccessful, provided some additional information. The presence of a similar compound from sample E and F at $R_f = 0.70$ has already been noticed in Figure 4.11 with the 3:2 $MeCN/H_2O$ mixture. The TLC analysis with the 1:9 and 1:12 $EtOAc$ /pentane solvent mixture from Figure 4.13 shows the presence of a compound in sample E only. When looking back at Figure 4.15, this unique compound is most likely eluting at the solvent front. Thereby, the spots present at the solvent front for sample 5 and F are not displaying the same compound as sample E. The fact that 5 and F share a similar compound and not sample E has also been noticed in Figure 4.12 for nearly all $EtOAc/CHCl_3$ ratios.



Figure 4.16. TLC of sample F co-spotted with chloranil and maleic anhydride. The label "D" was a more purified version of sample 5 that will be explained in the following section.

To allow the rise of further speculations on the multiple compounds present in the samples, the 5:3:1:1 eluent was modified to see if some other compounds may elute better. Four modifications were performed with the addition of one unit of pentane, one of EtOAc, one of H₂O, and two of EtOAc. Figure 4.17 depicts the modified systems with the incorporation of the regular system at the far right for reference.

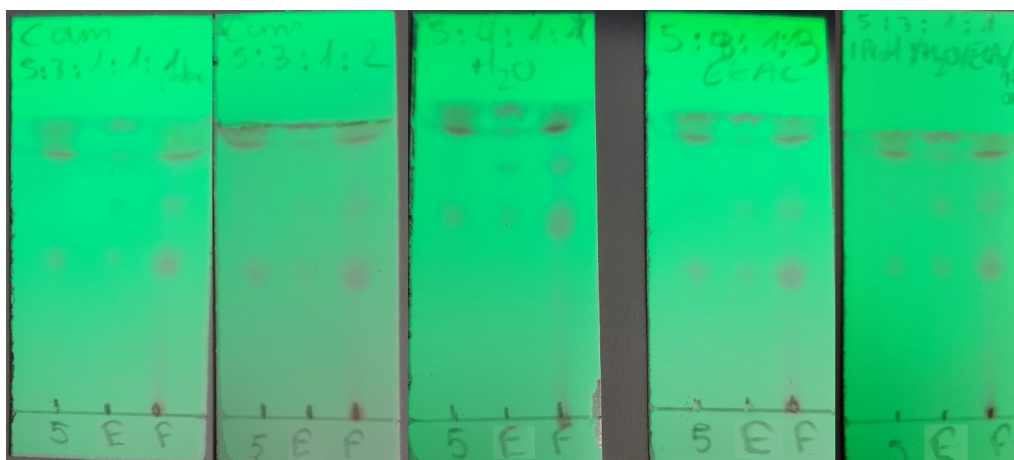


Figure 4.17. TLC of sample 5, E, and F with five different eluent systems from the 5:3:1:1 mixture. From left to right, the systems include one added unit of pentane, one of EtOAc, one of H₂O, two of EtOAc, and the regular system.

The first element readily noticeable is the presence of this double solvent front for all the plates similarly to Figure 4.11 with the 3:2 ratio of MeCN and H₂O. The fact that this phenomenon is still occurring for the reference plate at the far right confirms that this did not happen from the additions of solvent units into the mixture. The only difference from this batch of eluent to the one used in Figure 4.15 is time. Several weeks went by and the mixture had only been mixed slightly by twirling the 100 mL blue cap glass bottle containing the eluent before developing the TLC plates. The different solvents may have vaguely separated, causing a segregation in elution when looking at the solvent front. This

unexpected event did, however, shed light to an interesting fact. When looking at these two fronts for each sample, one can see a minute difference in spot intensity for sample E compared to sample 5, and F. This may, by chance, be an indication that the top spot for sample E is in fact not the same compound as the one for sample 5 and F. That being said, this remains an indication.

The addition of one unit of pentane seems to have increased the distance between the two solvent fronts when compared to the reference TLC plate. Increasing the unit of EtOAc by one or two seemed insignificant for the compounds. Water had the opposite effect as pentane. As a whole, it shifted the position of all compounds a little further towards the top. The overall end goal was to either lift the compound eluting at the baseline of sample F or drop the ones eluting at the solvent front of all samples. As this was not achieved through the several modifications, the original 5:3:1:1 eluent system was considered to be the most efficient one for separation through liquid column chromatography.

4.2.4 Additional Purification Steps

First and foremost, the samples are quite unprepared for the column. The multiple TLC, and post-reaction steps did impact the volume of the samples. Sample 5 and F had a large volume from the 300 and 150 mL of 2:1 EtOAc/CHCl₃ used for them respectively. Sample E, on the other hand, was dried in a rotary evaporator from 150 mL to around 5 mL as mentioned in Section 4.2.2 where it was thought that the product would not recrystallize due to too low concentration. In response, sample E was diluted by adding 5 mL of solvent and the total volume of sample 5 and F was reduced to around 17 g, or about 26 mL of solution. Note that sample F had the remained black dust that easily went through the hot filtrations. When evaporating sample 5, small crystals quickly started to appear at around 45 mL of solution. A picture of such crystals is shown in Figure 4.18.



Figure 4.18. Picture of sample 5 after evaporation through a rotary evaporator. The orange solution displays some orange solids floating at the surface and in the bulk of the mixture.

These solids are most likely the same solute dissolved in the solvent giving rise to this orange color. It is quite unlikely that this was an insoluble compound that was insoluble from the beginning but small enough not to be seen. Regardless, collecting these solids and spotting them on a TLC plate would answer this question readily. The suspension was attempted to be collected via a regular plastic and metal spatula and some fresh solvent was poured on the spatula and down to a beaker where a TLC was performed. The solution remained colorless and the TLC plate displayed no spots. A regular gravity filtration was performed and the residue was not washed but rather transferred into a beaker with some fresh 2:1 EtOAc/CHCl₃. The ability of the solvent to either dissolve or simply move the solute into said beaker was irrelevant as it was only needed for the solids to be separated from the rest of the original filtrate. This, unfortunately, failed as well. The issue might lie with the very fine distribution of the solids dispersing through the medium preventing it from efficiently separating them for the liquid part. Removing the liquid or reducing its volume would increase the ratio of the solid present in it. Evaporating the sample further would only increase the chance of further polluting the solution with impurities. Hence, centrifugation was performed.

The centrifuge used was a Sigma 3-16L model from 2016. The entirety of the content of sample 5 was transferred into a 50 mL polypropylene (PP) 28 x 114 diameter to length tube placed into a 13 104 round-bucket centrifuge rack with a maximum rotor size of 15.5 cm. The solution was balanced with the appropriated amount of water and centrifuged at the maximum speed of 5 000 rpm for 5 minutes. With this speed and rotor size, the relative centrifugal force (RCF) reached 4 340 x g. The resulting vial displayed a clear separation between the now light orange supernatant and dark orange pellet. The supernatant was carefully decanted using a pipette and transferred into another vial. The resulting pellet was around 1 mL and the supernatant 30 ml, which is quite odd. Unfortunately, the mass was not kept track. It is possible that the pellet might have absorbed some of the supernatant due to the high centrifugal force applied. 25 mL of fresh 2:1 EtOAc/CHCl₃ was poured into the pellet to re-dissolve it for TLC. This however was proven to be impossible as the pellet in question was insoluble in said solvent. This is a promising fact as this means that the solute dissolved in the solution is not the same compound as the pellet. To back this statement, the supernatant and the residue now suspended in 2:1 EtOAc/CHCl₃ were spotted on a TLC plate with the same 5:3:1:1 eluent system determined earlier in Section 4.2.3. Figure 4.19 shows the resulting sheet with the residue and supernatant labelled "5s" and "5l" respectively.

It is clear now that the pellet is indeed immiscible with 2:1 EtOAc/CHCl₃. The pellet also displays a very peculiar orange color, quite similar to perylene. However, not only have earlier TLC results shown the absence of perylene in all samples, but perylene is also readily soluble in CHCl₃ and should in theory partially mix with CHCl₃ despite the presence of EtOAc to which perylene can not dissolve into. For further contradiction, perylene anhydride has a red color. [38] A picture of the fully evaporated suspended residue is displayed in Figure 4.20 below. Xylene did not dissolve the pellet either. Hence, another solvent was sought upon.



Figure 4.19. TLC of sample 5s and 5l with 5:3:1:1 i-PrOH/H₂O/NH₃/EtOAc as the mobile phase.

Perylene anhydride is often further reacted to yield an imide and in this context, the anhydride is dissolved in dimethylformamide (DMF). [36, 38] Dissolving the pellet in this solvent and spot it afterwards would serve as an optimistic indication of the presence of the anhydride. Sample 5s was fully evaporated under vacuum and 10 mL of DMF was poured into the Florentine flask, causing the pellet to fully dissolve as expected.

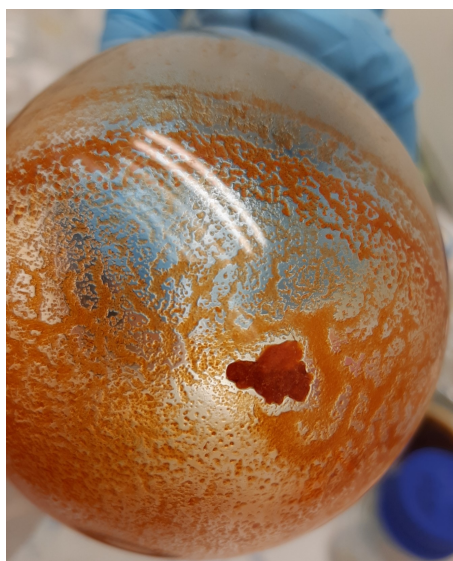


Figure 4.20. Picture of sample 5s after fully evaporated under vacuum. The solids have a distinct orange color with some red aggregates.

The residue dissolved in DMF is labelled "5s2". The now dissolved residue and the supernatant were spotted on a TLC plate and Figure 4.21 depicts the result. Two plates were developed as it was thought that the first one was not performed correctly. No dots were seen for 5s2 beside a rough blur at the solvent front even though the residue is most definitely dissolved in DMF. The reason behind this may come from the fact that the boiling point of DMF is 153 °C, which is very high knowing that the solvent has to fully

dry before starting the elution. This was expected initially and the spots were left to dry for nearly 5 minutes more than any other solvents prior to running the TLC plates, but this has shown to be unsuccessful.

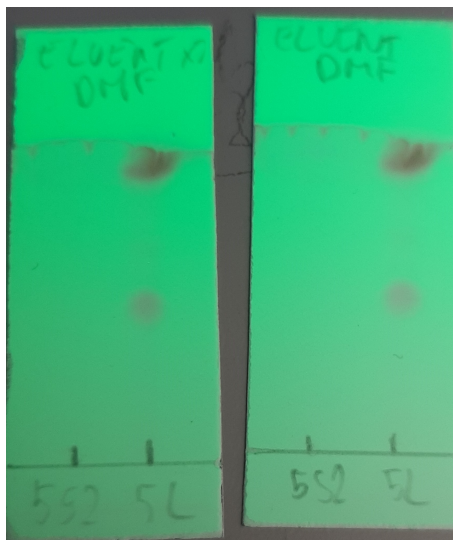


Figure 4.21. TLC of sample 5s2 dissolved in DMF and 5l dissolved in 2:1 EtOAc/CHCl₃. The mobile phase remained the same.

If the sample is indeed impossible to be spotted on a TLC plate, the use of a column seems more trivial. As concluded by Figure 4.16, the middle compound seen for sample 5l is maleic anhydride, or its acid form. In this case, and knowing the difference in solubility of maleic anhydride from the rest of the components, separating them based on their solubility seems a lot more promising than a column. That being said, targeting the solubility of maleic anhydride without disrupting the rest would lead to a decent first separation step. Maleic anhydride is readily soluble in water but also reacts to form maleic acid, which was thought to potentially be a problem for the perylene product, since it also harbors an anhydride group. Instead, EtOH was used. 5l was dried under vacuum and about 20 mL of EtOH was poured in. EtOH was allowed to extract as much as the maleic anhydride as possible for about 10 min. After that, the suspension was still very well dispersed through the medium, and the sample was yet again centrifuged with the same parameters as earlier. This time, however, the pellet had much more trouble sitting down the tube, and would rather remain in suspension. Regardless, the resulting pellet and supernatant of sample 5l were yet again spotted on a TLC plate. The two samples harbored the exact same spot implying that either the residue remained too dispersed into the medium or the EtOH extracted nearly everything from the evaporated 5l sample.

Despite this, as the use of EtOH seemed inconclusive, water was tried as well. The 5s2 pellet was insoluble in 2/1 EtOAc/CHCl₃, thus another hydrophobic solvent was sought and ironically, CHCl₃ dissolved the pellet readily. The perylene anhydride is insoluble in such solvent which indicates the absence of such product in the pellet. Nevertheless, the extraction was performed as intended. The pellet was transferred into a separatory funnel along with enough CHCl₃ to reach 10 mL and 10 mL of water was added. The funnel was gently shaken and vented 4 times or until no gas came out. The mixture was left to sit for 30 min, and the organic bottom layer was collected as well as the aqueous top one. In

general, aqueous layers sit at the bottom as water is often much denser than most organic solvents, but chlorinated solvents are the exceptions. This step was performed twice.

The solution from the organic and the solution from the aqueous phase are labelled "O₂" and "A₂" respectively. These two are spotted in a TLC plate with the same eluent and on old TLC sheet done before the washing steps is put on the left for comparison. The resulting pictures are shown in Figure 4.22.

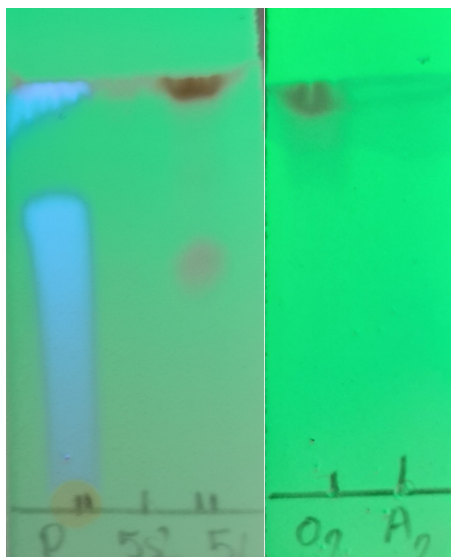


Figure 4.22. TLC of sample O₂ and A₂ next to an old TLC sheet of sample 5s2, 5l, and perylene for reference.

This comparison allows us to realize that the wash has indeed removed maleic anhydride as seen on the O₂ spot. While the maleic anhydride is not seen on the A₂ sample, it is very possible that the high boiling point of water caused the same effect as DMF earlier.

To maximize water extraction, the O₂ sample was dried under vacuum once again and suspended with 20 mL of water for 10 min. The content was filtered through gravity filtration and both the residue and filtrate were collected. The residue was re-dissolved in 5 mL CHCl₃. The TLC showed no compound present in the filtrate which was also implied by its transparent color. Even if the extraction worked, the top compounds remains unknown until any assumption is made upon which compound should elute at.

Hence, with the elements brought by the eluent system, it is possible to start speculating on the association of the compounds to the spots visible on the TLC plate, instead of trying to target the compounds one by one. The correlation is detailed in Figure 4.23. In almost all cases, the higher up a compound elute, the lower its polarity. The stationary phase, that is silica gel, harbor very polar hydroxide groups, inducing strong forces between itself and the polar compounds. Consequently, polar compounds tend to elute at the bottom of the plate as it interacts strongly with the hydroxide groups of the silica gel. On the other hand, a non-polar compound will ignore such interactions and move along the mobile phase more readily. Influencing the polarity of the mobile phase will not re-order the compounds, but rather shift the whole set of dots further towards the solvent front, or the baseline.

Based on the possible outcome of the reaction and their known polarity, one can determine their placement on the sheet. The dots labelled "1" are most likely chloranil as they eluted at the same rate as the chloranil co-spot. Additionally, chloranil plays the role of an oxidizing agent in this reaction, meaning that its chemical structure and amount should remain intact. Spot number "2" shares a similar polarity as chloranil, but as discussed earlier, evidences state that sample E harbor another compound than sample 5 and F. This compound might be the coronene dianhydride formed as a side-product of the Diels-Alder reaction. Its symmetry renders this molecule non-polar. Compound number "3" is most likely the aimed product. This is rather logical as, when looking at its chemical structure, its polarity is higher than chloranil and coronene dianhydride due to its anhydride group, but lower than maleic anhydride due to its six aromatic rings. Compound 4 and 5 are then maleic anhydride and its acid form respectively.

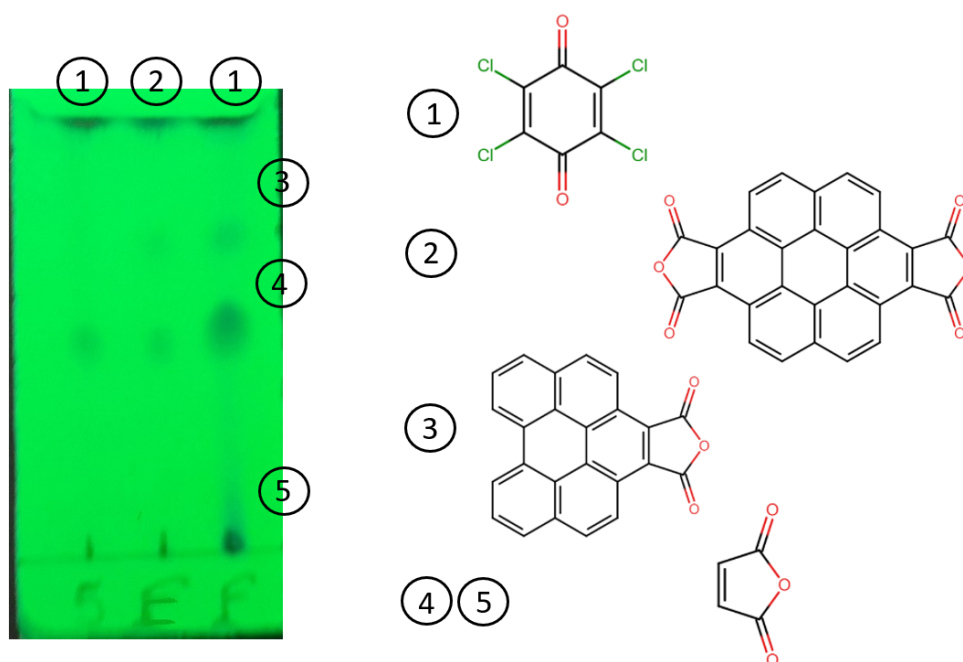


Figure 4.23. Scheme including a TLC sheet with numbered speculated compounds for each dots.

That being said, chances are that sample 5 never had the perylene product to begin with, and the focus should be shifted towards sample E and F. Based on the methodology, sample 5 results from the poor extraction of the solids from xylene at the very first purification procedure. Whilst the hot filtration and the rest of the protocol was performed correctly a second time, the fact that xylene was only warmed to 35 °C and used once reduces drastically the extraction potential. Performing the rest of the purification steps is pointless if the product had not been extracted in the first place. As sample F has a much higher amount of the targeted compound and volume, additional purification will be performed on it before sample E. A gravity filtration setup was made to remove the black dust present in the dark red solution. The solution was then dried under vacuum. A picture of sample F before and after evaporation is displayed in Figure 4.24.



Figure 4.24. Picture of sample F before and after dried under vacuum.

The sample depicts a dark orange/red color. As perylene anhydride is immiscible with CHCl_3 , about 50 mL of CHCl_3 was poured into the dried sample. In theory, most of the impurities should dissolve in the solvent, leaving the aimed product in suspension, or stuck to the side of the glass. The content of the flask was then passed through a vacuum filtration. However, no residue was seen on the filter paper. It was thought that maybe the particles of perylene anhydride were so small that they could pass through the filter with the help of the vacuum. Consequently, a regular gravity filtration was performed as well, which also failed to collect any solids. The solution had a similar color as Figure 4.24, and no suspension or solids were noticeable. This issue confirms that the perylene anhydride seemed to not have been successfully synthesized during the reaction. If some formed, it may have been left in the black mud leftover from the initial flask, or lost in some of the manipulation for the purification process. Although the synthesis seem to have failed for this particular compound, it would seem that an orange product which is not perylene nor the anhydride product, had been synthesized. This compound may very well be the coronene dianhydride, which partially explains its solubility in CHCl_3 .

The long time period used for both the reaction and purification procedure may have resulted in too much available time for the maleic anhydride to react with the synthesized perylene anhydride to form the coronene version. This would have been avoided if the reaction times were respected, and the purification quickly performed. On top of that, the entirety of the reactor flask should have mixed around or broken with a rod to allow all of it to transfer into the filtration setup. The entirety of the first purification manoeuvre could have also been optimized and performed in a more efficient way, similar to the second time. The mass of the lost maleic anhydride stuck in the condenser should have also been measured to know how much did not react in the reaction. The closer the value to its initial mass, the lower the amount of synthesized product. Finally, the temperature did not reach $240\text{ }^\circ\text{C}$ which is crucial for solid-state reflux reaction. Solids failed to efficiently react with one another, it was, hence, critical for the temperature to be way above the boiling point of maleic anhydride.

5 Non-Vinyl Polymerization

5.1 Suzuki Cross-Coupling: Experimental Methods

5.1.1 Suzuki Cross-coupling Polymerization

The protocol used in this experiment was derived from the work of Kumsampao et al. [39]. The chemical equation for the polymerization is shown in Figure below. The ratios of every reactants remained similar to those of the article.

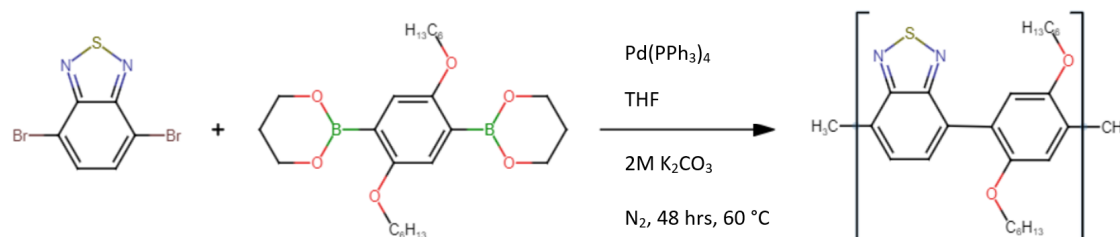


Figure 5.1. Chemical equation of the Suzuki cross coupling polymerization of 4,7-dibromobenzo [c][1,2,5] thiadiazole and 2-[4-(1,3,2- dioxaborinan-2-yl) -2,5-dihexylphenyl] -1,3,2-dioxaborinane into the benzothiadiazole and dihexylphenyl polymer. Reaction conditions from [39].

The monomers were from our lab products. 101.7 mg ($3.50 \cdot 10^{-4}$ mol) of 4,7-dibromobenzo[c][1,2,5]thiadiazole along with 322.0 mg ($7.22 \cdot 10^{-4}$ mol) of 2-[4-(1,3,2-dioxaborinan-2-yl)-2,5-dihexylphenyl]-1,3,2-dioxaborinane, 10 mL of 2M K₂CO₃ (≥ 99.0 % Sigma-Aldrich[®]), and 20 mL of THF were added into a 250 mL two-headed round flask assembled into a reflux setup. A drawing and an actual picture of the setup is displayed in Figure 5.2. The system was then pumped and purged with nitrogen gas for about 10 minutes three times.

Simultaneously, 27.1 mg ($2.35 \cdot 10^{-5}$ mol) of tetrakis (triphenylphosphine) palladium(0) (≥ 97.0 % TCI[®]) complex was weighted out in a glass beaker and an additional 10 mL of THF along with the catalyst. The solution was added into the system quickly to not allow all the nitrogen from the balloon to run out. The reaction proceeded at 60°C for 48 hours. The size of the balloon is also monitored to assess whether any gas leakage is noticeable and a picture of the mixture is taken occasionally.

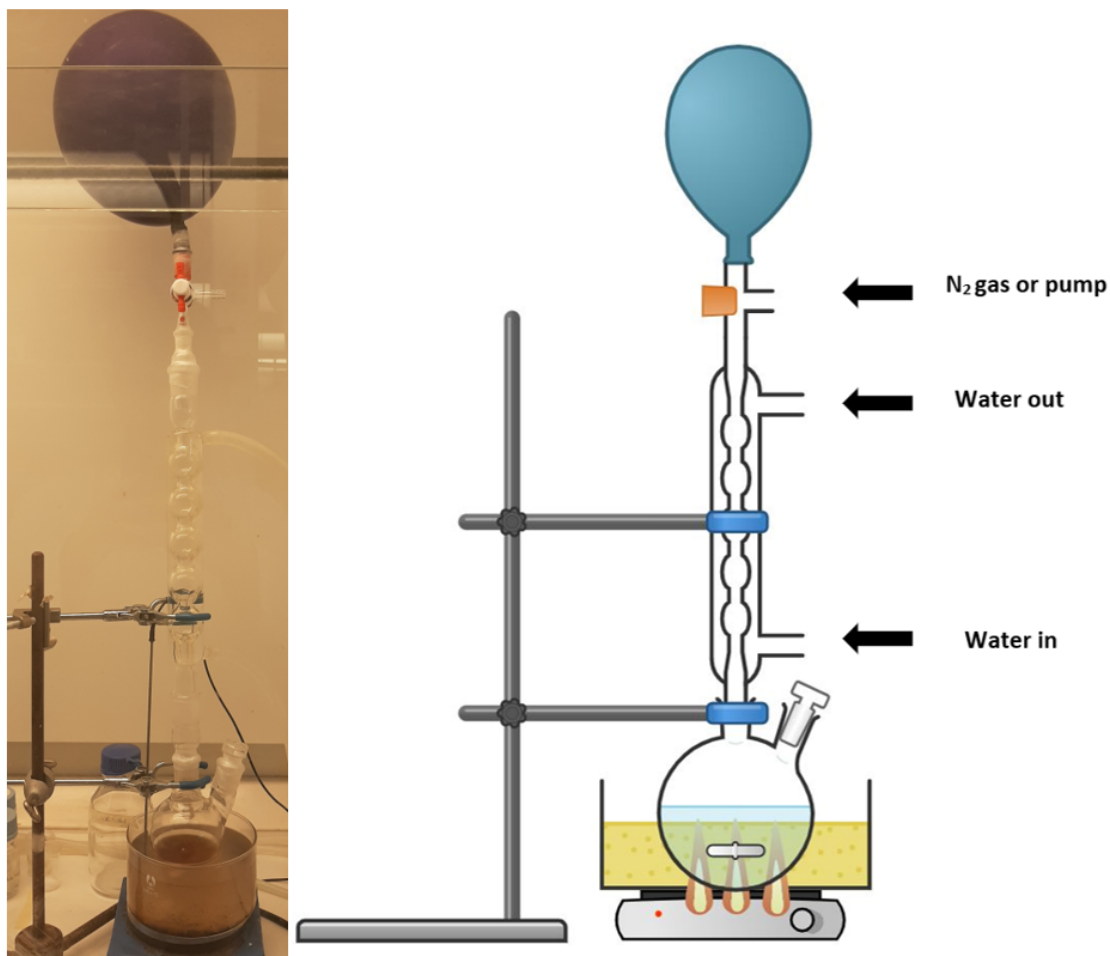


Figure 5.2. On the left is a picture taken of the setup for the Suzuki cross-coupling polymerization with a schematic drawing on the right. This setup is identical even throughout the emulsion experiments.

The viscosity seemed to have increase by the 24 hours mark. After 48 hours, the reaction was stopped and allowed to cool down to room temperature. The solution turned much darker after 48 hours as opposed the start of the reaction. To assess the ability of the polymer to precipitate with a polar solvent, 1 mL of the mixture was dropped in water, MeOH and acetone. MeOH seemed to allow the clearest precipitation to occur. The main source taken from the protocol do not induce a polymerization reaction and thus another separation/purification was seeked upon. [40] The separation and purification protocol is presented in Figure 5.3 below.

50 mL of MeOH was poured into the flask which caused the mixture to turn from dark brown orange to red instantly, and the content was vacuum filtrated. The residue present on top of the filter was rinsed with some fresh MeOH, acetone, and distilled water. Unfortunately, rinsing the solid with distilled water caused it to dissolve entirely, passing through the filter and falling into the receiving Erlenmeyer flask. This was concerning as the polymer should be relatively non-polar. The content of the Erlenmeyer flask was transferred into a 500 mL evaporatory flask and all of the solvent was dried entirely.

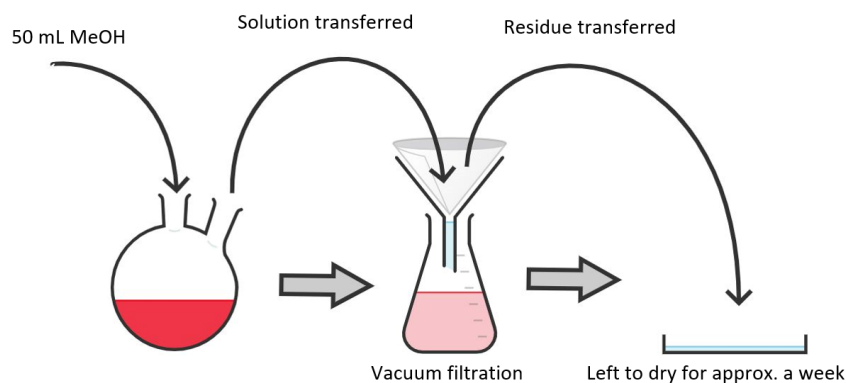


Figure 5.3. Separation and purification process first performed for the Suzuki cross-coupling polymerization. The solid left in the dish was easily transferred into a 10 mL glass vial without having to scrape the plate.

The flask was then redissolved/suspended in fresh MeOH and once again vacuum filtered without rinsing the residue with water. Note that the insoluble solid from the evaporatory flask was collected by scraping the side with a glass spatula as they were stuck to the side of the glass. The residue was then put in a glass dish covered with parafilm with holes and left to dry for about a week. The whole batch was then transferred into a small glass vial. A picture of the resulting sample is shown in Figure 5.4.

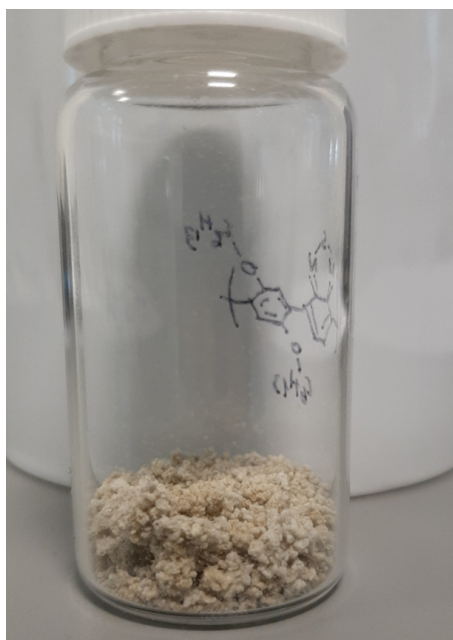


Figure 5.4. Dried product from the Suzuki cross-coupling polymerization performed as a pilot project for the emulsion polymerization. The product has a grey/brown color.

The final mass was exactly 1.0288 g. With a total mass of 0.4237 g from the reactants, the resulting solid has a 242.8 % yield indicating the presence of a large amount of impurities. Further characterization will provide more insight into the product's actual content. The solid seemed relatively insoluble in chloroform but an NMR analysis was tried nonetheless, as the two monomers were also relatively non-soluble as well, yet gave clear NMR data.

5.1.2 First Suzuki Cross-coupling Emulsion Polymerization

The same setup as the pilot project was constructed for the emulsion polymerization with the exception of the surfactant tween 80 (Sigma-Aldrich®), the use of a liquid nitrogen bath and a lifter. For this reaction, the protocol was inspired from the work of Wang et al. [41]

In a 250 mL two-headed round-bottom flask, 33.8 mg ($1.15 \cdot 10^{-4}$ mol) of 4,7-dibromobenzo[c][1,2,5]thiadiazole along with 64.3 mg ($1.44 \cdot 10^{-4}$ mol) of -[4-(1,3,2-dioxaborinan-2-yl)-2,5-dihexylphenyl]-1,3,2-dioxaborinane were added with enough toluene to dissolve the mixture. One milliliter was added at the time up to 10 mL but the mixture did not seem to dissolve as well as the source stipulates. Then, the mixture was frozen with liquid nitrogen after sealing the setup. The setup was pumped out and purged with nitrogen three times before thawing the mixture for about 30 minutes. This cycle was repeated three times. As the atmosphere was controlled with a balloon full of nitrogen, 100 mL of 2M K_2CO_3 was added into the flask. The remaining solid base stuck in the beaker was dissolved in approximately 5 mL of water and poured once again into the flask. The tween 80 was relatively difficult to collect via a pipette. It was calculated that 5.5 mL of the non-ionic surfactant should be added into the flask but the pipette could not gather all the viscous liquid at once, thus, it was gathered and added twice from a 5 mL pipette which adds up to approximately 6 to 6.5 mL. finally 10 mg ($8.65 \cdot 10^{-6}$ mol) of $Pd(PPh_3)_4$ dissolved in a bit of toluene was added into the flask. The oil bath was heated to 90 °C and the rotor speed of the magnet was set to 700 rpm. The reaction was left to run for 48 hours. The reaction darkened slightly at the end of the reaction time. The mixture was left to cool to room temperature before separation. The chemical procedure for the separation and purification is clarified in Figure 5.5.

50 mL of toluene was added into the flask, the stirring was set at 1100 rpm and the reaction was allowed to run for 10 min. The solution was then transferred to a 500 mL separatory funnel where the aqueous layer was separated from the organic one. Interestingly, a black interlayer was present between the two surfaces and was kept in the organic phase. An additional 100 mL of water was added to remove extra aqueous content from the aqueous phase. However, this caused the solution to blur instantly, hindering any separation. 50 mL of toluene was added and the solution was left to sit overnight. After 24 hours, the solution had separated once again and the organic phase was collected once more and dried under pressure without additional washing steps.

The toluene was fully evaporated and some solid was visible on the side of the reactor flask, however, an orange viscous liquid of about 1 mL was still present and thought to be leftover surfactant. With that in mind, 15 mL of MeOH was poured into the flask which caused the liquid to dissolve in it, leaving the solids. As some suspension was noticed, the MeOH was carefully decanted. This step was performed three more times until added MeOH appeared crystal clear. The flask was dried and filled with 200 mL $CHCl_3$. This turned the chloroform slightly cloudy and grey. The flask was then put in a ultrasonic bath for over 80 min. When done, the content was transferred into 4 separated glass dishes using extra chloroform, methanol, and ethanol to dry for about 24 hours.

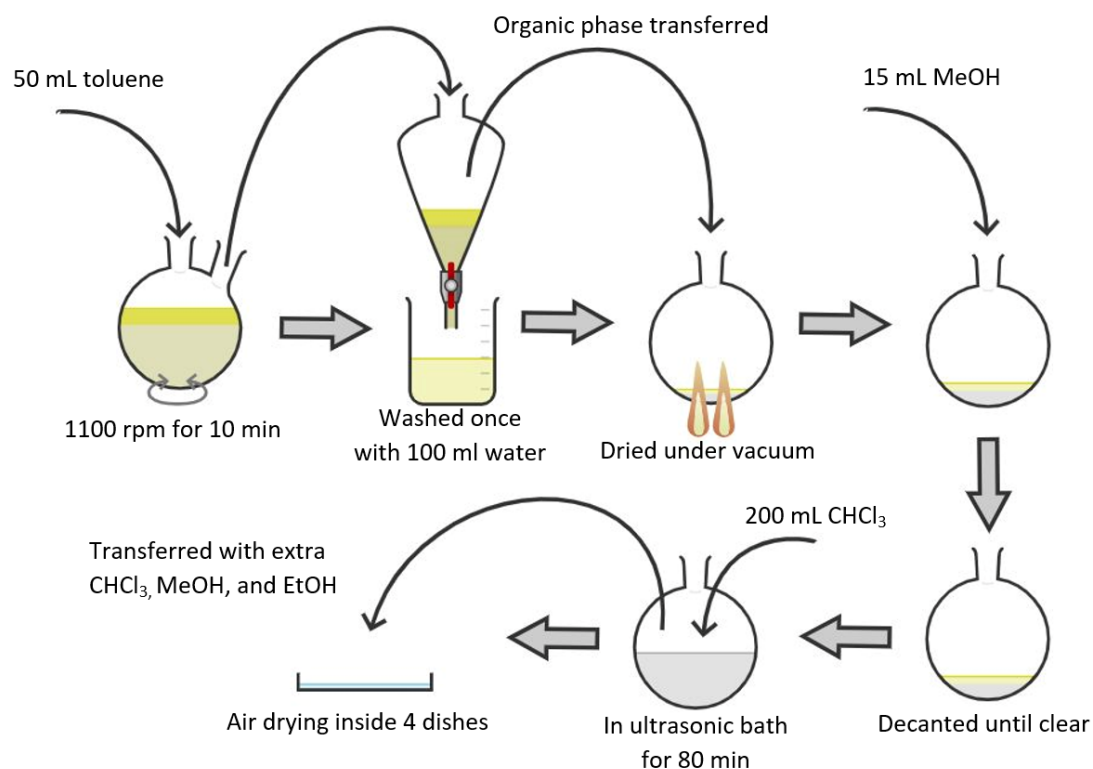


Figure 5.5. Separation and purification process first performed by the first Suzuki cross-coupling emulsion polymerization. The dried solid from the four dishes were collected via a metal spatula.

When completed, the solid was scraped and the content transferred into a small 10 mL glass vial. It was noticed that some particles were distinctly light brown and others were white. As they were from same dishes and thus difficult to separate by hand, they were all transferred to the same vial. The resulting product can be seen in Figure 5.6. The final mass was 280.7 mg. With an expected mass of 98.10 mg, the sample has a 286.1 % yield, showing yet again the presence of large amount of impurities. This correlates with the difference in color from the particles harvested off the dishes. Further characterization will provide more insight into the product's actual content. Similarly to the precedent experiment, the sample looked insoluble in chloroform, yet NMR was still performed.

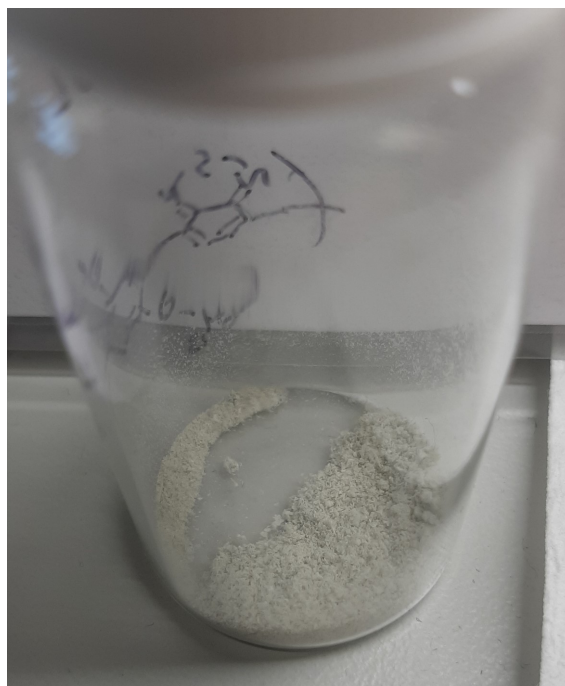


Figure 5.6. Dried product from the first Suzuki cross coupling emulsion polymerization performed. The overall powder has a grey/white color.

5.1.3 Second Suzuki Cross-coupling Emulsion Polymerization

The methodology was similar to the first emulsion polymerization with some exceptions. The volume ratio of toluene to water from the initial protocol was 1:25. This was done to aim a nanoparticle size of 100 to 200 nm. [41] However, according to a patent work from Cambridge Display Technology (CDT) [31], the ratio should range from 1:1 to 1:10 preferably for optimal results. With that in mind, the ratio of solvent for this emulsion polymerization was aimed to 1:1. Thus, 103.9 mg ($2.33 \cdot 10^{-4}$ mol) and 83.9 mg ($2.85 \cdot 10^{-4}$ mol) of the same dihexylphenyl and benzothiadiazole monomers were added into a beaker with 1.78 mL of toluene and stirred for 10 min. The monomers poorly dissolved in toluene even for such long stirring. Hence, the content was transferred as it was with an additional 5 mL of solvent.

The tween 80 was difficult to transfer to the reactor for the first emulsion reaction. This time, the required amount of aqueous base was poured into a beaker and the surfactant was added until the mass confirmed the complete transfer. Then, the beaker was put on a stirring plate and the content of the beaker was poured into the flask when the surfactant seemed to have fully dissolved. However, tween 80 remained hard to transfer into the round flask as it did not dissolve entirely in the aqueous base even after around 5 min of stirring. Thus, the surfactant was scooped with a metal spatula into the flask with the help of a small amount of the aqueous base used. Similarly with toluene, the volume of aqueous base rose from 1.78 mL to 6.78 mL to ease the transfer. Note that the molarity of the aqueous base was adjusted accordingly. After purging the system with nitrogen gas and hindering the evaporation of any solvent via cycling between freezing, pumping, and purging with liquid nitrogen three times, 17.2 mg ($1.50 \cdot 10^{-5}$ mol) of the tetrakis (triphenylphosphine) palladium(0) was added. The schematic recapitulation of the separation and purification

process is depicted in Figure 5.8.

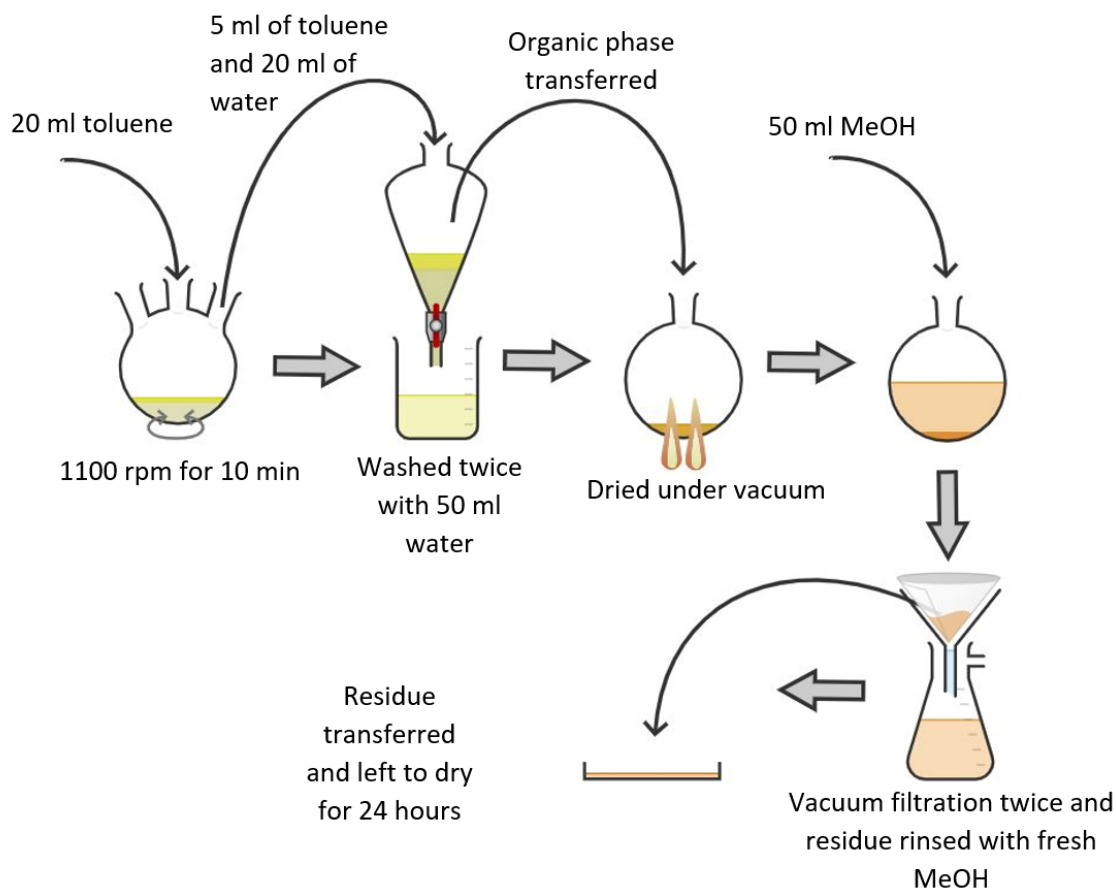


Figure 5.7. Separation and purification process performed by the second Suzuki cross-coupling emulsion polymerization.

Once the reaction was over, the mixture was allowed to set to room temperature. Then, 20 mL of toluene was poured into the three-necked flask, and the stirring was set to 1100 rpm for 10 min. The content of the flask was transferred into a 250 mL separatory funnel with roughly 5 mL toluene and 20 mL distilled water. The content was shaken gently, however, an emulsion still occurred similarly to the previous experiment. The bilayer was set to separate for about 1 hour. The aqueous layer was discarded, and 50 mL distilled water was poured into the separatory funnel for an additional wash. After an hour, the bilayer formed once again and the lower aqueous layer was discarded. The solution was washed once more with water. It was hoped that the organic phase would turn from bright yellow to a grey/brown blur, but this did not occur. The organic phase was collected into a 50 mL evaporatory flask to dry under vacuum.

To transfer the organic phase into the evaporatory flask, additional toluene was added. Toluene, unfortunately, seemed to be immiscible with the organic top phase. This is quite concerning, so the aqueous phase was kept as well. Chances are that the emulsion was still quite present, preventing the extraction of the polymer into the toluene. The procedure was continued nonetheless. After drying the sample, 50 mL of MeOH was added to dissolve any remaining aqueous substances. The solvent immediately turned yellow and the orange

solid stuck to the side started to suspend with the MeOH. As there seem to be a lot more in suspension, the flask was not sonificated but rather vacuum filtrated. The residue was rinsed with MeOH and the filtration was performed twice as some of the orange residue fell into the filtrate, The two filter papers were let to dry for 24 hours in a glass dish covered with parafilm. The resulting orange solids, seen in Figure 5.8, were particularly difficult to transfer into the 10 mL glass vial due to their extreme stickiness.



Figure 5.8. Dried product from the second Suzuki cross coupling emulsion polymerization performed. The product has an orange color.

The final mass was around 9.8 mg, out of the 187.8 mg from the monomers, the product has a yield of 5.2 %. This is quite the opposite result from the two precedent experiments. Note that a minor fraction of the product remain stuck to the side of the petri dish which may account for 1 mg or less. The product was used as it was for further characterization. As another contrast, this sticky solid was readily soluble in chloroform.

5.2 Suzuki Cross-Coupling: Results and Discussion

After the reaction, three samples were available for characterization. The first sample from the regular Suzuki cross-coupling polymerization is labelled sample "0", the next one about emulsion polymerization is labelled sample "1", and lastly the final emulsion polymerization is labelled sample "2". To perform the difference analysis, a suitable solvent has to be found to dissolve each product. As Nuclear Magnetic Resonance (NMR) was to be performed on all three products, CHCl_3 was poured on a small fraction of each sample. Interestingly, only sample 2 showed significant solubility, which is in accordance with its orange color, often translating to a high degree of conjugation. Several solvents were tried on sample 0. All of them are shown in Figure 5.9. Sample 0 was insoluble in CHCl_3 ,

chlorobenzene, EtOAc, MeCN, pentane, and dichlorobenzene, but readily soluble in water. This was also noticed in the methodology section earlier. Sample 1 was also readily soluble in water. As the product is not supposed to be soluble in water, this property seems to confirm the synthesis of yet another product. Regardless, ultra-violet/visible (UV/vis) spectroscopy, and fluorescence spectroscopy were performed to analyze the products' optical and fluorescence properties. Next, NMR and infrared (IR) spectroscopy were performed to investigate the chemical structure of the samples. Lastly, dynamic light scattering (DLS) was done to assess the change in particle sizes.

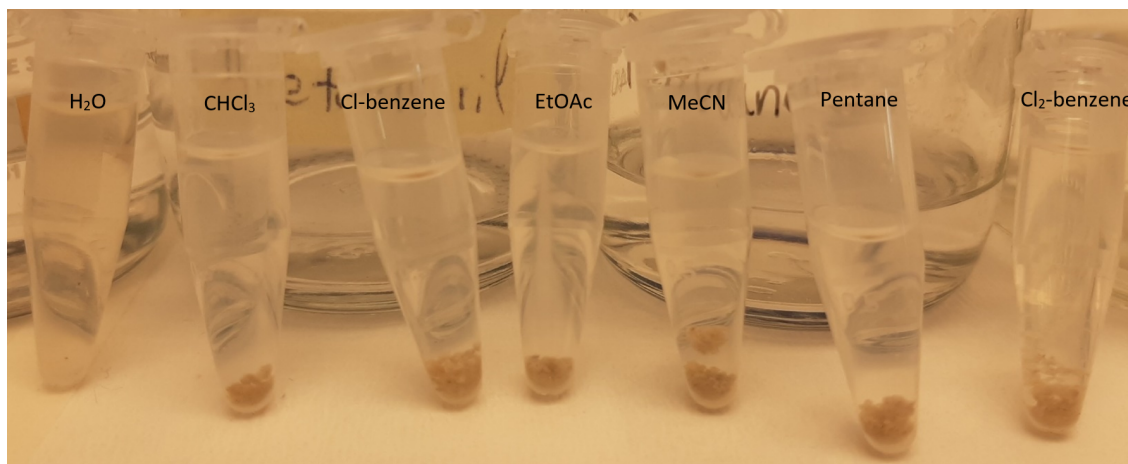


Figure 5.9. Picture of sample 0 in 7 different solvents.

In 20 ml disposable scintillation vials, an arbitrary amount of the three samples were dissolved in their respective solvent. As the cuvette could contain a maximum of 4.2 ml, 3.0 ml of solvent was estimated to be a decent volume. Respectively, 22 mg and 13 mg of sample 0 and 1 were dissolved in 3 ml of water, whereas only 1.3 mg of sample 2 was dissolved in CHCl_3 , as its stickiness and small yield made it complex to transfer more. The solutions had a concentration of 7.3 mg/ml, 4.3 mg/ml, and 0.43 mg/ml for sample 0, 1, and 2 respectively.

5.2.1 UV/Vis Spectroscopy

The samples were measured on a Varian Cary 50 Bio spectrophotometer third version. The scan rate was 600 nm/min between 200 to 800 nm. The beam mode was set to dual beam. Each samples had a baseline correction based on their solvent. As the absorbance was in the UV range, a QS Hellma[®] quartz cuvette with 10 mm light path was used. Sample 2 reached absorbance level way higher than one and was consequently diluted 20 times. The reduced concentration reached 0.022 mg/ml. The outcome for all three samples is shown in Figure 5.10.

Sample 0 and 1 hold one peak at around 260 nm and 315 nm respectively, whereas sample 2 holds two of them, one at 310 nm and one at 420 nm. The area before 250 nm for sample 2 seems to either be noise or issues regarding CHCl_3 and the quartz cuvette. All three samples have absorption peaks in the UV range with the exception of the second peak of sample 2 at 420 nm, majorly responsible for its yellow color.

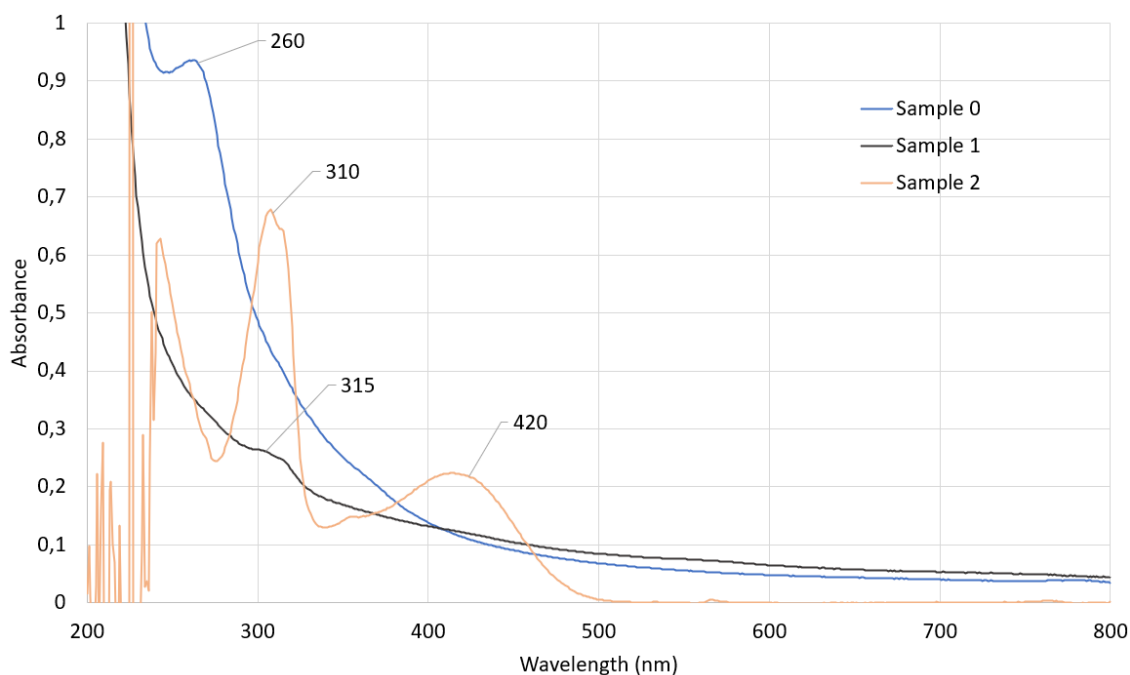


Figure 5.10. Absorption spectra of all three Suzuki cross-coupling products.

To some degree, all three graphs display different absorption. Sample 1 and 2 do share a peak at around 310 nm but this absorption is minute in sample 1, maybe due to a low concentration. The difference in color of all three samples hinted at their different nature. Their absorption spectrum seems to confirm this fact

5.2.2 Fluorescence Spectroscopy

The measurements were done using a Varian Cary Eclipse fluorescence spectrophotometer. The scan rate was set to 600 nm/min and the wavelength range was set depending on the emission and excitation range. As the emission is always higher in wavelength than the excitation, the nanometer range was adjusted accordingly. The PTM voltage was set to medium. A QS Hellma[®] fluorescence quartz cuvette with a 10 mm light path was used. A fluorescence cuvette has all of the sides transparent. An estimation of the excitation wavelength of each sample was determined through the UV/vis spectra provided in the previous section. The spectrum for the maximum emission and excitation wavelength is displayed in Figure 5.11 below.

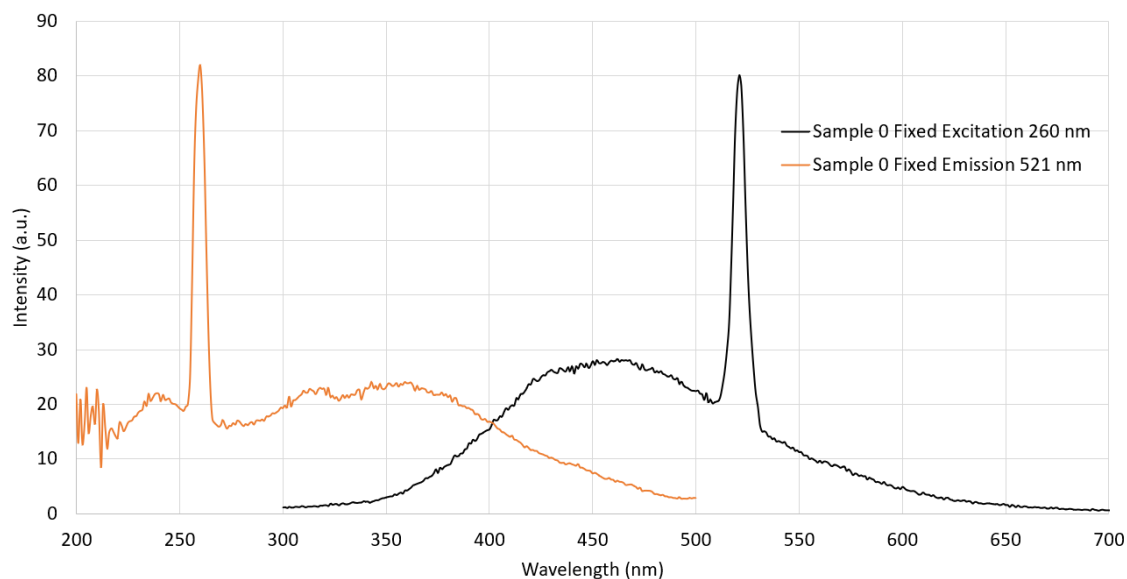


Figure 5.11. Fluorescence spectrum of sample 0. The maximum emission spectrum is shown on the right, and the maximum excitation wavelength spectrum is shown on the left.

The maximum emission wavelength of sample 0 is located at around 521 nm. When plotting that value to give the spectra of maximum excitation, the same excitation value is given. The Stoke shift between the two maxima is 261 nm.

The same spectrum is shown for sample 1 in Figure 5.12. Here, the emission spectra was fixed by the previously determined excitation wavelength.

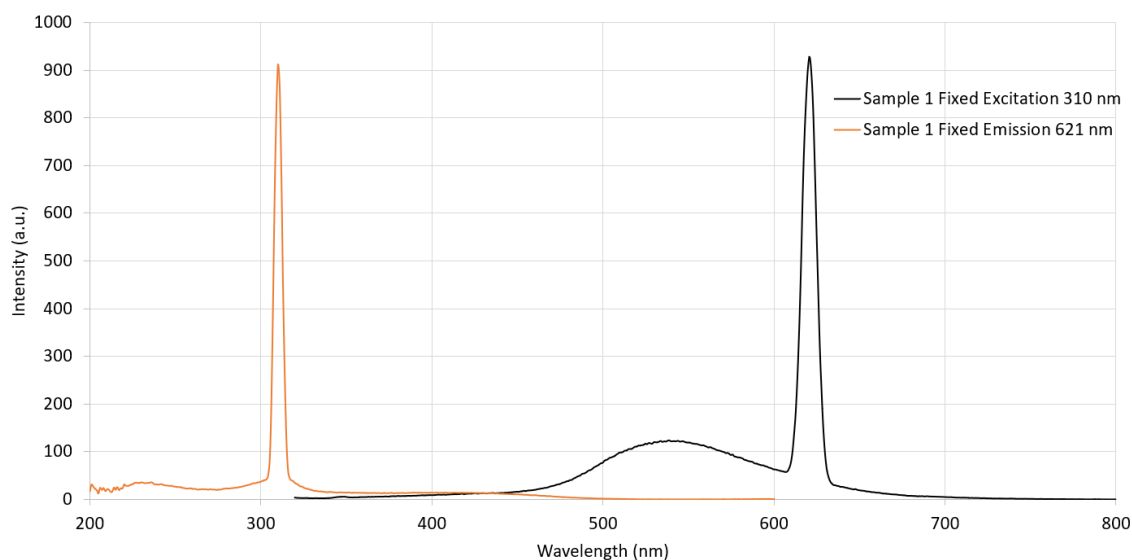


Figure 5.12. Fluorescence spectrum of sample 1. The maximum emission spectrum is shown on the right, and the maximum excitation wavelength spectrum is shown on the left.

The shape of the maximum emission spectrum of sample 1 looks like sample 0. Though the emission values differ. The Stoke shift of sample 1 reaches 311 nm. Lastly, the fluorescence spectrum of sample 2 is depicted in Figure 5.13.

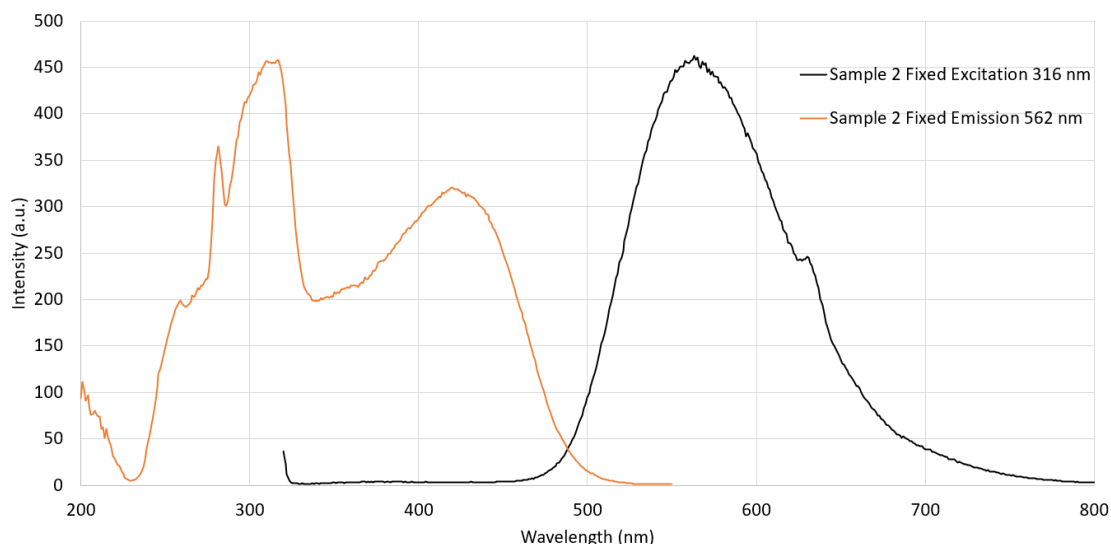


Figure 5.13. Fluorescence spectrum of sample 2. The maximum emission spectrum is shown on the right, and the maximum excitation wavelength spectrum is shown on the left.

As already shown by the UV/vis spectrum of sample 2, several excitation signals are present. The Stoke shift here reaches 246 nm, which may also have been influenced by the change in solvent.

5.2.3 Dynamic Light Scattering

Dynamic light scattering (DLS) measurements were done using a zetasizer nano-series model ZEN3600 from Malvern Instruments Limited[®]. The refractory index was set to polystyrene and the solvents were input manually. To prevent the effect of concentration of the solute upon the particle size, a series of 5 solutions for each sample were prepared for DLS. The vials containing the solution of the three samples used for characterization were used for the dilutions. From there, 0.5 ml of solution was transferred into a 2 ml Eppendorf tube along with 1 ml of water for sample 0 and 1 and CHCl_3 for sample 2. The tube was mixed by hand, and using a vortex mixer for around 10 seconds. Then, 0.5 of that diluted solution was transferred into the next tube and the process was repeated until 5 Eppendorf tubes were made for each sample, totaling 15 tests. If the concentration is too high the particle sizes will tend to become higher, if that concentration is too low, the sizes will become noisy with high variation. The purity of the data did not meet the quality control of the DLS and some z-averages were outliers to the set of data. These outliers can be seen through the large error bars mainly for sample 1. The graphs for each sample are shown in Figure 5.14.

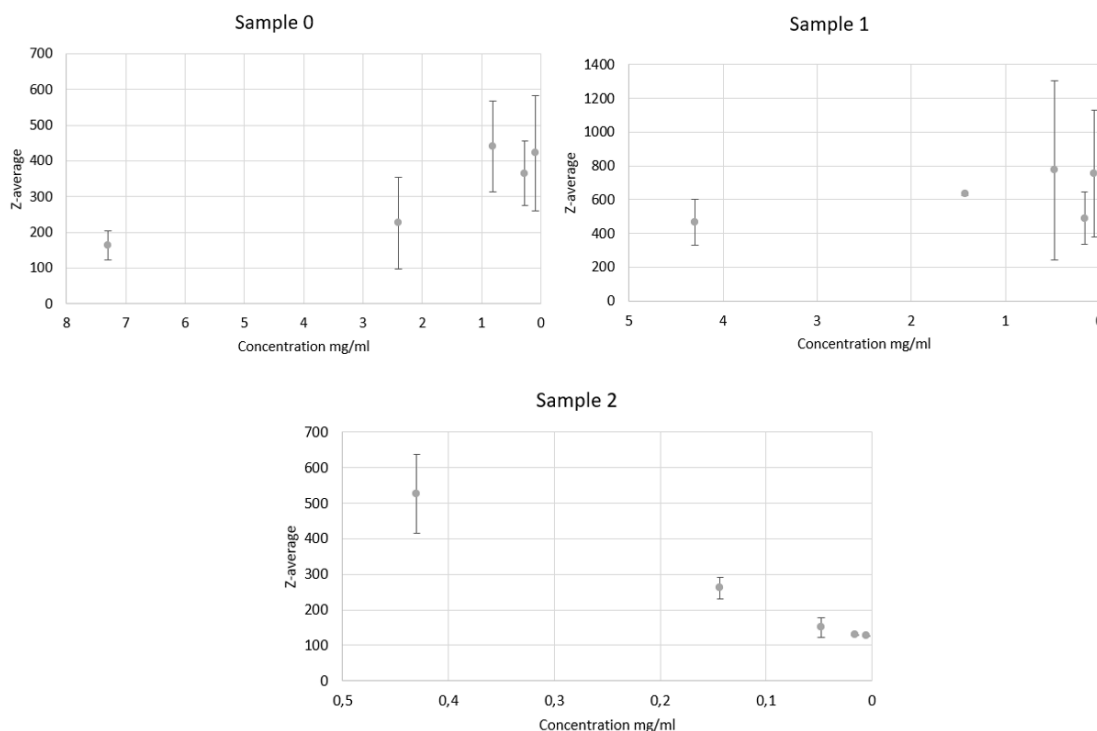


Figure 5.14. DLS measurement for all three samples. The Z-average is plotted against the concentration. Each data point had three measurements and are thus displayed by averages along with their standard deviation.

The noise effect induced by a low concentration is readily noticeable for sample 0 and 1 where concentrations under 1 mg/ml increased drastically the standard deviation of the averages. This is the opposite for sample 1 where the initial concentration yielded a high z-average. If one was to select the average particle size from each graph, sample 0 has a particle size around 163 nm, sample 1 around 465 nm, and sample 2 around 126 nm.

In terms of size distribution, all three samples seem to have similar results. The main difference is their particle size. The first emulsion yielded a drastically bigger particle size than both the regular polymerization and the second emulsion. In fact, the first emulsion polymerization had a lot more solvent per monomer ratio than the second emulsion to allow very small micelle formation, but this seemed to have failed. One can speculate that the reaction did not reach completion or that the amount of solvent saturated the environment and prevented the monomer from polymerizing in the micelles but rather in the medium. With a much smaller amount of solvent per monomer, the particle size was reduced as seen for the second emulsion. Chances are that the polymerization was allowed to occur in the micelle when the environment was not saturated by the aqueous solvent.

5.2.4 Infrared Spectroscopy

The IR spectra were obtained using a Bruker® Fourier-Transform IR Tensor II instrument with a platinum attenuated total reflectance (ATR). The background and sample single channel measurements were performed with a 128 scan time as opposed to the regular 64 scan time. The wavenumber x-axis range 400 cm^{-1} to $4\,000\text{ cm}^{-1}$. Table 5.1 depicts the

type of bonds along with their frequency and intensity for the expected polymer product. Their values were used from the fifth edition of "Introduction to Spectroscopy" by Pavia et al. [42]

Table 5.1. List of bonds present in the polymer product with their frequency and intensity.

| Type of bond | Frequency (cm^{-1}) | Intensity |
|------------------------------|--------------------------------|-------------|
| O-H (H-bonded) | 3400-3200 | medium |
| C-H sp^3 stretch | 3000-2840 | strong |
| C-H sp^2 stretch | 3095-3010 | strong |
| C-H ₃ bend | 1450-1375 | medium |
| C-H ₂ bend | 1465 | medium |
| C-H sp aromatic stretch | 3150-3050 | strong |
| C-H sp aromatic out-of-plane | 900-690 | strong |
| C=C aromatic | 1600-1475 | medium/weak |
| C=C alkene | 1680-1600 | medium/weak |
| C-O ether | 1300-1000 | strong |
| C=N imine | 1690-1640 | strong/weak |
| C-Br | <667 | strong |

Figure 5.15 shows the IR spectroscopy graph of sample 0. Each type of bond expected to be shown is displayed with its wavenumber and label.

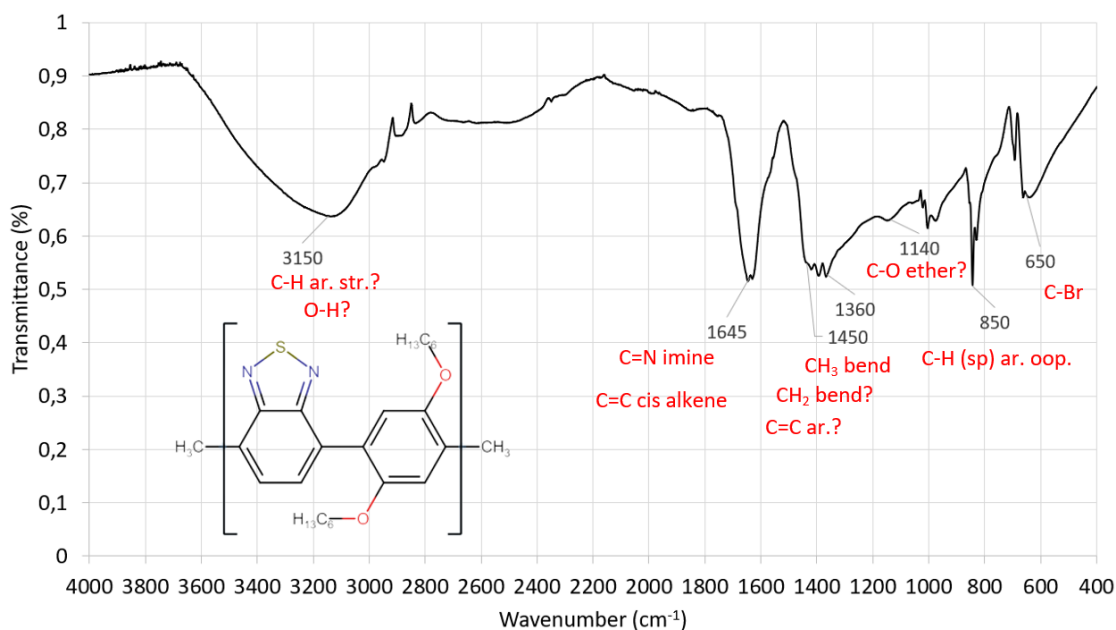


Figure 5.15. IR graph of sample 0. The type of bond listed in Table 5.1 is labelled and noted within the graph. The expected polymer is drawn on the bottom left corner of the graph.

The first element noticeable from the graph is the broad peak located at around 3150 cm^{-1} . While its location is around the same as the C-H aromatic bond, its broadness is very indicative of a O-H bond. A C-H aromatic bond would display a sharp and strong signal at this range, which is still possibly occurring, but masked by the O-H signal. A

reasonable interpretation for this overlapping is most likely the lack of proper drying steps after the synthesis. Even though the product was left to dry for a week under a fume hood, this is far from being as effective as using an oven. The next peak is located at 1645 cm^{-1} and can correspond to both a C=N imine or a C=C cis alkene signal. The intensity of a C=C alkene signal is stronger when in cis configuration and in this particular graph, a strong signal seems to show at 50% of transmittance. In other words, both signals can be located at that area. The signal for a C=C aromatic is concernedly not present or not as present as it should be. There is a slight bump on the left part of the peak at 1450 cm^{-1} that may translate to such a bond. However this signal remains very mild. Next, the C-H sp^2 is also on the edge of that peak and is difficult to efficiently determine. That is not the case for the C-H sp^3 signal showing a distinct peak in the appropriate area. The C-O ether bond from the dihexylphenyl-dioxaborinane monomer displays a very mild signal at 1140 cm^{-1} . This is in contradiction with the commonly strong intensity of such bond, as listed in the table. The next signal is at 850 cm^{-1} and is most likely a C-H sp aromatic out-of-plane signal, typically representative of a para configuration for substituted aromatic rings, which is the case for both monomers of the copolymer. The ortho and meta configuration of the dihexylphenyl-dioxaborinane monomer seem to be absent in the graph as well. Lastly, a medium broad signal is shown at 650 cm^{-1} , and this can be correlated to unreacted or end-chained benzothiadizaole monomer. Despite all these indications, the most distinctive indication is the lack of C-H sp^3 and C-H sp^2 signals. All in all, the benzothiadizaole is present in sample 0 based on the IR graph. That can not be as easily determined for the second monomer. The only signal indicative of its presence is the one for C-H sp^3 . However, without the C-H sp^3 and C-H sp^2 stretch signals, its absence is certain. This will be further concluded via NMR. The graph for sample 1 is shown in Figure 5.16 below.

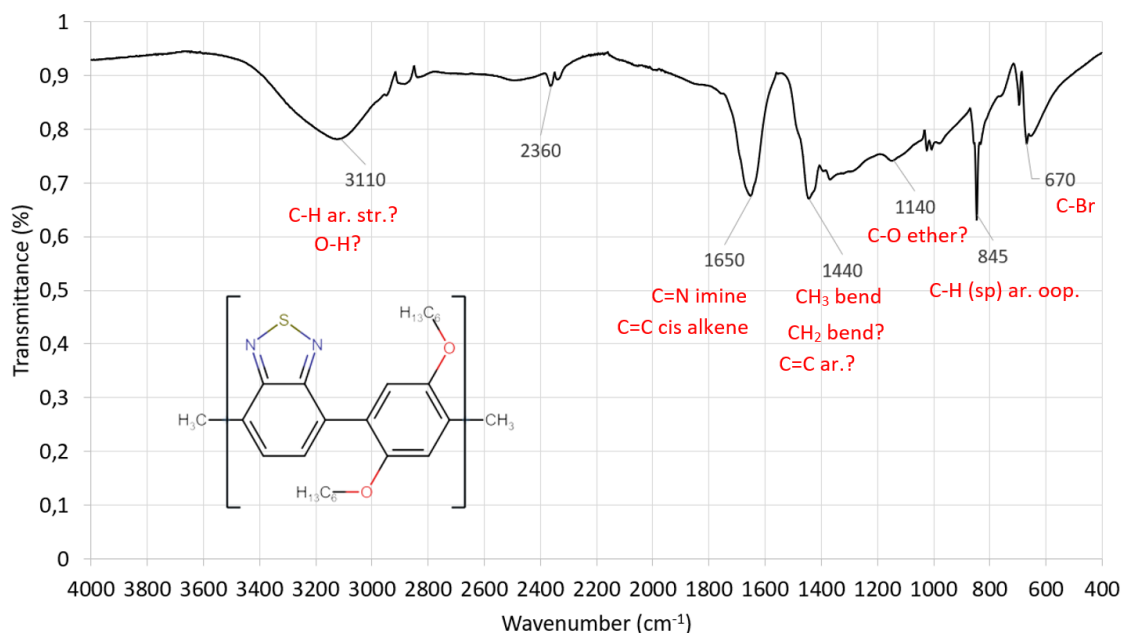


Figure 5.16. IR graph of sample 1. The type of bond listed in Table 5.1 is label and noted within the graph. The expected polymer is drawn on the bottom left corner of the graph.

The similarity in physical property, such as color and solubility, between sample 0 and 1 is proven by their nearly identical content. The graph for sample 1 is nearly identical to sample 0 with a few exceptions. Firstly, the signals seem generally weaker than sample 0. Secondly, the signal for C-H sp^2 and C=C aromatic is a lot less obvious than the previous graph. Here only the signal for C-H sp^3 at 1440 cm^{-1} is seen. Lastly, a weak signal is observed at 2360 cm^{-1} which can not be associated with a particular bond. The two graphs seem to agree on the presence of benzothiadiazole and the absence of the boronate monomer. The graph for the third and final product, sample 2, is shown in Figure 5.17.

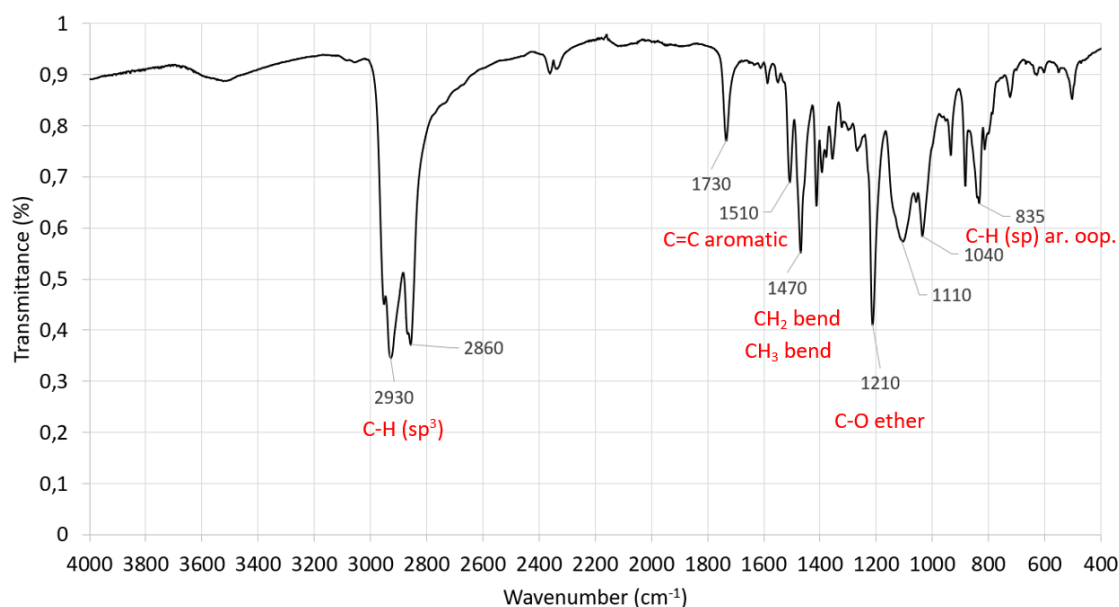


Figure 5.17. IR graph of sample 2. The type of bond listed in Table 5.1 is labelled and noted within the graph. The expected polymer is drawn on the bottom left corner of the graph.

Sample 2 has already stood out from the two other samples by its color, solubility, and stickiness. The IR analysis confirms this difference. Here, a strong signal for a C-H sp^3 stretch is seen at 2930 cm^{-1} . The presence of the aliphatic chain of the boronate monomer is also proven by the medium CH₂ and CH₃ bend signals at 1465 cm^{-1} , rounded up to 1470 cm^{-1} in the figure, and around 1440 cm^{-1} respectively. The C-O ether bond is shown at 1210 cm^{-1} with a relatively strong intensity. However, the C=N imine signal shown in the two previous graphs seems absent in the third graph. While the IR analysis on the first two samples seems to reveal the presence of the benzothiadiazole monomer, the last IR analysis on sample 2 seems to reveal the dihexylphenyl-dioxaborinane monomer.

5.2.5 Nuclear Magnetic Resonance

The instrument used was a Bruker[®] Avance II with 600 MHz. Tetramethylsilane (TMS) is used as the reference. Each of the samples were dissolved in an appropriate amount of CDCl_3 for ^1H NMR. The approximate chemical shift ranges from the expected functional groups of the products are shown in Table 5.2.

Table 5.2. List of the approximate chemical shift range for the functional group of the product copolymer.

| Functional group | Chemical shift (ppm) |
|----------------------|----------------------|
| R-CH ₃ | 0.7-1.3 |
| R-CH ₂ -R | 1.2-1.4 |
| R-O-H | 0.5-5.0 |
| R-O-C-H | 3.2-3.8 |
| Benzene | 6.5-8.0 |

The first graph for sample 0 is shown in Figure 5.18.

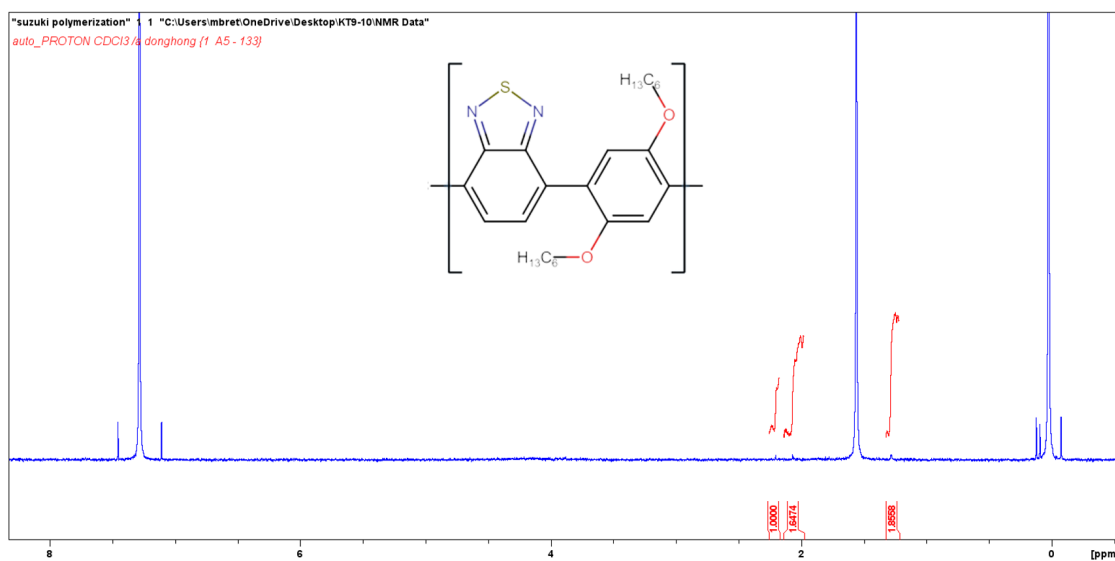


Figure 5.18. ¹H NMR graph of sample 0 with the integrals of each signal. The y-axis has been zoomed in for better resolution of the signal.

Starting from the far left, a signal is present at around 7.3 ppm, located at the exact range of the CDCl₃ solvent. However, the triplet nature of this signal, hints that it may hide a benzene signal. Yet, if the monomers were correctly synthesized and polymerized, a doublet from the benzothiadiazole or singlet from the dihexylphenyl-dioxaborinane would have been shown in this chemical shift range. Instead, the signal depicts a proton attached to a benzene ring having two other protons neighboring it. This would, in theory, be possible if the benzothiadiazole would harbor a hydrogen instead of an end-chain expected bromide. A nucleophilic substitution would also be possible if a base like sodium or potassium hydroxide was in solution. The hydrogen would remain shielded by the oxygen, however. Water is not a strong nucleophile, but with enough time and exposure such substitution is possible. Nonetheless, a doublet signal should also be noticeable on the spectrum if such reaction occurred.

The insolubility of sample 0 in CDCl₃ is quite clear when looking at the graph. This insolubility may be due to polymer rigidity or high molecular weight. The two strong signals at 1.5 ppm and 0 ppm belong to water, already hinted by the IR analysis, and TMS. NMR requires high concentration of the solute for efficient analysis. The very minute solubility of the product is also shown by the absence of peaks for the compound in

question. The resolution of the y-axis has been extended to see if any peaks are noticeable despite the noises. Three small signals can be noticed from 2.2 to 1.2 ppm. Due to their limited size, it is difficult to interpret them as singlet, doublet or any split peaks. The next ^1H NMR graph is shown in Figure 5.19.

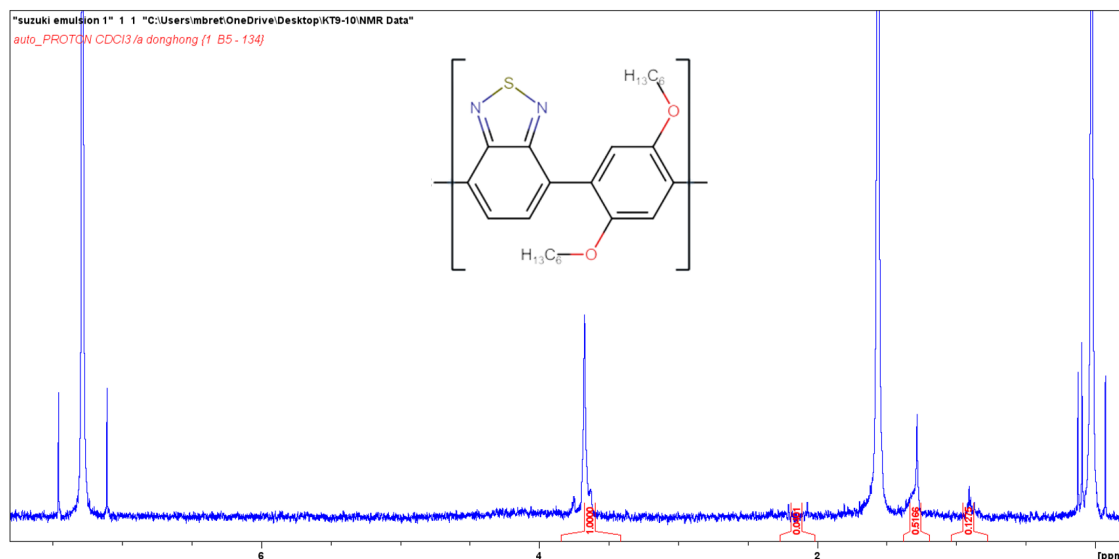


Figure 5.19. ^1H NMR graph of sample 1 with the integrals of each signal. The y-axis has been zoomed in for better resolution of the signal.

The ^1H NMR spectrum of sample 1 shows similarities with sample 0. The two small signals at 2.2 and 2.0 ppm from sample 0 are also present for sample 1. The signal at 1.2 ppm is also present yet stronger for sample 1. There is also a supposedly triplet at 3.6 ppm and a singlet at 0.9 ppm. The chemical shift of the triplet at 3.6 ppm matches the value of a R-O-C-H bond. The proton from this bond also has 2 neighboring protons and thus should exhibit a triplet signal. The results from the IR analysis, however, do hint at the absence of such groups and as the IR is arguably more reliable than NMR spectra from insoluble compounds, chances are that this signal may illustrate a hydroxide group from a possible nucleophilic substitution. The IR spectra hinted at the presence of the benzothiadiazole which should have resulted in signals located around 8.0-6.5 ppm. This signal may be again hidden by the CDCl_3 signal. Yet again, solubility can be blamed.

The similarity in the ^1H NMR spectra between the two samples is backed up once again by their comparable IR spectra and physical properties. The difference in UV/Vis and fluorescence spectroscopy does hint at some chemical group differences. The fact that both sample 0 and 1 are water soluble is most likely due to the excess aqueous base used in the polymerization reaction. Additionally, on account of the surfactant, removing said base from the organic phase via separation was relatively complex and that is yet shown in the results here. The presence of organic compounds in such hydrophilic environment may be issued by a drastically small amount of the product surrounded by the base. This way, the powder looks soluble in water but remains in suspension in nanometer range. The poor quality of the NMR spectra of sample 0 and 1 could have been avoided by using D_2O instead of CDCl_3 . The ^1H NMR of sample 2 is depicted in Figure 5.20.

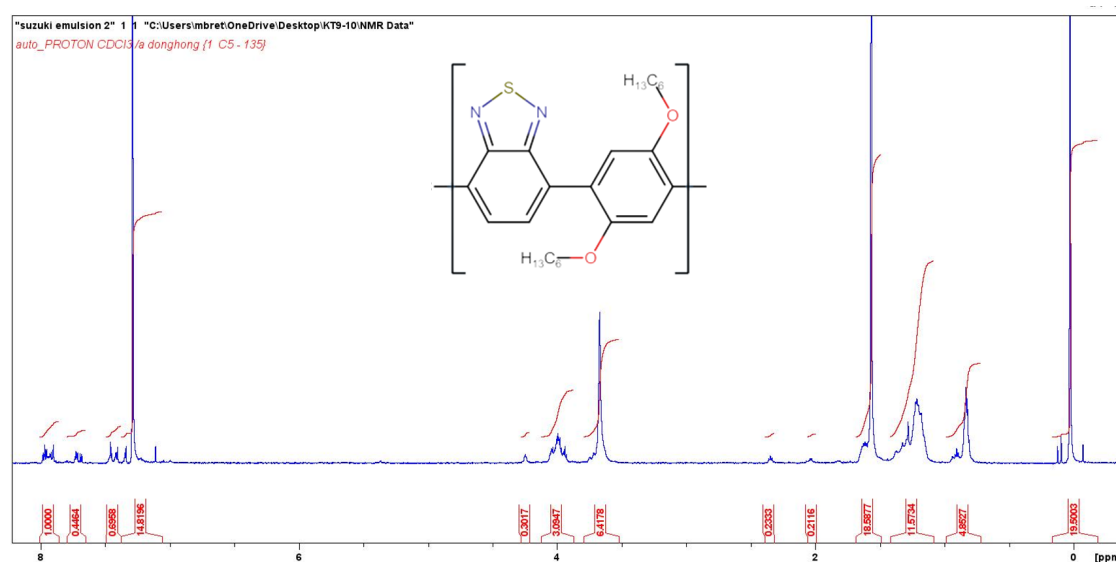


Figure 5.20. ^1H NMR graph of sample 2 with the integrals of each signal. The y-axis has been zoomed in for better resolution of the signal.

The spectrum is, as expected, presenting different signals when compared to sample 0 and 1. According to the IR analysis, the dihexyl-phenyl-dioxaborinane monomer is present in sample 2, but the dibromobenzothiadiazole is not. The first element seen in this NMR spectrum is the relatively low intensity of the peaks, implying a low concentration despite the high solubility. The signals from 1.4 ppm to 0.7 ppm are identical to sample 1 yet stronger in intensity. The aliphatic chains are expected to be shown through triplet, five or six multiplets as the protons located through the chain have 2, 4, and 5 neighboring protons. The triplet is expected to be in the 1.3-0.7 range and the rest at the 1.4-1.2 ppm range. For better resolution, a zoomed in picture of the areas are displayed in Figure 5.21.

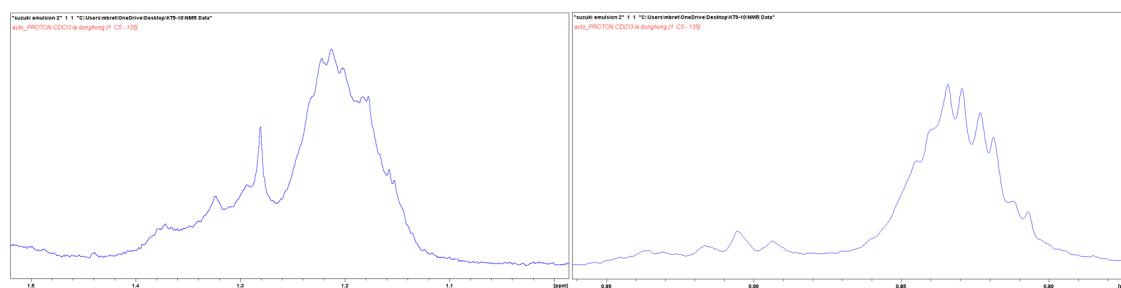


Figure 5.21. ^1H NMR graph of sample 2. The signals from the left graph range from 1.5 to 1.0 ppm, whereas the signals from the right graph range from 1.0 to 0.75 ppm.

The signals on the left graph seem to agree with the expected overlapping shape of multiplets of $-\text{CH}_2-$ in the area. Similarly, the signals on the right graph depict multiplets of what seem to be a quadruplet rather than a triplet. Regardless, this is mostly a result of signals overlapping once more. A triplet is expected to be shown from 3.8 to 3.2 ppm from the R-O-C-H bond. There, indeed, is a signal in this area. Whether this signal is a triplet or any other multiplet is harder to determine. Singlets are also expected from the 8.0-6.5 ppm range for the protons of the benzene ring. Though signals are shown in this area, they

do not seem to be presented as singlet, but rather doublets or triplets. This interesting information may disclose the fact that the dihexyl-phenyl-dioxaborinane monomer is not coupled with anything, but rather presents hydrogen groups at the para location of the supposedly backbone of the polymer. The proton may have substituted with the boron end groups of the monomer.

When looking back and forth between the NMR spectrum of sample 1 and 2, similarities in their signals start to appear. Sample 1 also has the signal of R-O-C-H at 3.8-3.2 ppm and the ones from the aliphatic chain at 1.4-0.7 ppm. This indicates that if the water residue and most of the impurities were to be removed, there is a chance that the dihexyl-phenyl-dioxaborinane monomer was indeed present in sample 1 as well. Knowing that IR is hinting at the presence of the benzothiadiazole in the same sample, there is a possibility that the polymer was successfully made. An argument against this statement, on the other hand, is the absence of signals in the 8.0-6.5 ppm range in the NMR spectrum of sample 1.

The second emulsion presents a strong contrast in results when compared to the other samples. When looking at the methodology, the biggest changing factor is the change of the solvent ratio from a 1:25 toluene/water to a 1:1 ratio as a patent work was advising this range for better results. Even if both emulsions went through nearly the same separation process, the second emulsion did not require any water removal steps or at least not as strongly as the other ones. One unmentioned possible cause for such deviation in results is the possibility that the given monomers degraded over time and had their chemical structure slightly differing. This would have been determined if an IR was to be performed on them. Regardless, a focus on the aforementioned solvent ratio is a crucial element of emulsion polymerization.

6 Conclusion

The first monomer synthesis of vinyl copolymers for organic photovoltaic application, and the polymerization of donor and acceptor monomers via Suzuki cross-coupling mechanisms under emulsion was intensively investigated. The extensive TLC analysis and separation methods from the cycloaddition of maleic anhydride into perylene provided a valuable insight. For example, to seek an optimal outcome, one has to prioritize the use of an oil bath during the reflux, the use of an air condenser instead of a water one to avoid solidification of maleic anhydride and the loss of product, the utilization of a metal rod to scrape the end-product to transfer the content entirely for filtration, and the addition of an aqueous separation step to remove un-reacted maleic anhydride. The application of TLC analysis has shown to provide excellent vision into the purity and compound identification of the different stages of the synthesis and should be common practice for such reactions. The appropriate eluent system was found to be optimal in a highly polar environment with the 5:3:1:1 i-PrOH/H₂O, NH₃, and EtOAc system yielding the clearest results.

The optical, particle size distribution and structural properties of the polymerized products from the Suzuki cross-coupling reactions are provided. The three different methodologies yielded very different results. Both the regular polymerization and the first emulsion products were heavily contaminated by aqueous residues, indicating the need for an adequate and controllable water removal and basic residue purification step. The volume ratio of organic to aqueous solvent played a crucial role to the contrast seen on the second emulsion polymerization. From a 1:25 to a 1:1 toluene to water volume ratio, the yielded product had opposite optical and physical properties and its structure remained fundamentally different from the first two reactions. Under these parameters, it was also possible to attain an average size distribution of around 126 nm with low standard deviation. By prioritizing the focus on the solvent ratio, it is feasible to efficiently control the average particle size distribution of the yielded product.

The global commercialization and interest of organic solar cells are arguably one step away from completion. The photogeneration and electron conductivity properties locked by covalently bonding donors and acceptors via block copolymerization remains a concept that could potentially revolutionize the field of solar cells and transition research inventions into commercial usage. For this purpose, this work helped in optimizing the first reaction step of the vinyl polymerization of designed copolymers, as well as providing experimental information to obtain a controlled particle size distribution by emulsion polymerization for non-vinyl polymerization.

7 Perspective

The synthesis of the perylene anhydride could have been performed differently to yield better results. For the sake of understanding the reaction, a second attempt was not tried to avoid similar mistakes. With the current perspective, the second trial could be performed once again under the same condition mentioned in the conclusion. The reactor flask also had two of its heads plugged with rubber stoppers with one pierced having the temperature rod attached. The high temperature caused the interior part of the stoppers to melt, contaminating the mixture as well as potentially opening a hole for the vapor to exit. A glass stopper with a screwable exit for a temperature rod would have worked better. The black dust from sample F should have been kept and characterized via IR. If the results hinted at the presence of perylene anhydride, then the rest of the solidified black mud from the reactor flask would have been transferred and used. Regardless of the solubility of sample F, the sample should have been kept and used for further characterization despite the indications of failed synthesis. The amount of side-products, especially the symmetrical coronene anhydride, could have also been prevented if the separation step was performed quickly after. If the anhydride was indeed well synthesized, then the product would have been reacting with an amino long chain with a hydroxide end-group to yield a perylene imide through nucleophilic substitution. The hydroxide end-group would then be further substituted with a vinyl group and the polymerization would be induced afterwards. The same concept would have been performed another time with another monomer with more electron donating or accepting properties to make copolymers from both vinyl monomers. The emulsion polymerization could also have been optimized as stipulated in the conclusion. Rather than aiming for finite nano-particles, the methodology should have ensured that the emulsion polymerization was occurring despite aiming for larger particles.

When both vinyl and non vinyl copolymers were synthesized, their photogeneration and electron conducting properties would have been tested. The two materials would be compared by their PCE, fill factor, short circuit density, open circuit voltage, internal and external quantum efficiency, and dielectric constant. Additionally, factors involving the synthetic routes of these copolymers would be brought for comparison. Factors such as the use of toxic or expensive solvent, reaction steps, temperature, and time would also be used when comparing both materials.

Bibliography

- [1] U. N. E. Programme, “Emissions gap report 2021: The heat is on – a world of climate promises not yet delivered,” 2021-10.
- [2] U. D. P. United Nations Environment Programme, “Emissions gap report 2020,” 2020-11.
- [3] U. N. E. Programme, “Emissions gap report 2019,” 2019-11.
- [4] U. N. E. Programme, “Emissions gap report 2018,” 2018-11.
- [5] NREL, “Best Research-Cell Efficiency Chart,” 2021.
- [6] I. Rey-Stolle, “Fundamentals of photovoltaic cells and systems,” in *Solar Energy*, vol. 2, pp. 31–67, 2016.
- [7] M. Hiramoto, *Organic solar cells : energetic and nanostructural design*. Singapore: Singapore : Springer, 1st ed., 2021.
- [8] M. Riede, D. Spoltore, and K. Leo, “Organic solar cells—the path to commercial success,” *Advanced energy materials*, vol. 11, no. 1, pp. 2002653–n/a, 2021.
- [9] A. G. Yu, J. Gao, J. C. Hummelen, F. Wudl, and A. J. Heeger, “Polymer Photovoltaic Cells : Enhanced Efficiencies via a Network of Internal Donor-Acceptor Heterojunctions,” *American Association for the Advancement of Science Stable*, vol. 270, no. 5243, pp. 1789–1791, 1995.
- [10] H. Kim, S. Nam, J. Jeong, S. Lee, J. Seo, H. Han, and Y. Kim, “Organic solar cells based on conjugated polymers : History and recent advances,” *The Korean journal of chemical engineering*, vol. 31, no. 7, pp. 1095–1104, 2014.
- [11] K. Jin, Z. Xiao, and L. Ding, “18.69% pce from organic solar cells,” *Journal of semiconductors*, vol. 42, no. 6, pp. 60502–, 2021.
- [12] P. D. Topham, A. J. Parnell, and R. C. Hiorns, “Block copolymer strategies for solar cell technology,” *Journal of polymer science. Part B, Polymer physics*, vol. 49, no. 16, pp. 1131–1156, 2011.
- [13] A.-E. Becquerel, “Report on the electrical effects produced under the influence of solar rays,” *Proceedings of the Academy of sciences*, vol. 9, pp. 145–149, 1839.
- [14] M. Riordan and L. Hoddeson, “The Origins of the pn junction,” *IEEE Spectrum*, vol. 34, no. 6, pp. 46–51, 1997.
- [15] J. C. Bernède, “Organic photovoltaic cells: History, principle and techniques,” *Journal of the Chilean Chemical Society*, vol. 53, no. 3, pp. 1549–1564, 2008.

- [16] P. Choubey, A. Oudhia, and R. Dewangan, "A review: Solar cell current scenario and future trends," *Recent Research in Science and Technology*, vol. 4, no. 8, pp. 99–101, 2012.
- [17] S. Sharma, K. K. Jain, and A. Sharma, "Solar Cells: In Research and Applications—A Review," *Materials Sciences and Applications*, vol. 6, no. 12, pp. 1145–1155, 2015.
- [18] Y. Li, X. Liu, F.-P. Wu, Y. Zhou, Z.-Q. Jiang, B. Song, Y. Xia, Z.-G. Zhang, F. Gao, O. Inganäs, Y. Li, and L.-S. Liao, "Non-fullerene acceptor with low energy loss and high external quantum efficiency: Towards high performance polymer solar cells," *Journal of Materials Chemistry A*, vol. 4, no. 16, pp. 5890–5897, 2016.
- [19] Q. Liu, Y. Jiang, K. Jin, J. Qin, J. Xu, W. Li, J. Xiong, J. Liu, Z. Xiao, K. Sun, S. Yang, X. Zhang, and L. Ding, "18% efficiency organic solar cells," *Science bulletin (Beijing)*, vol. 65, no. 4, pp. 272–275, 2020.
- [20] Z. Lei, Z. Ming, X. Jinqiu, L. Chao, Y. Jun, Z. Guanqing, Z. Wenkai, H. Tianyu, S. Jiali, X. Xiaonan, Z. Zichun, Z. Rui, Z. Haiming, C. Chun-Chao, M. R. C. I, Z. Yecheng, N. Jenny, Z. Yongming, S. Yanming, and L. Feng, "Single-junction organic solar cells with over 19refined double-fibril network morphology," *Nature materials*, vol. 21, no. 6, pp. 656–663, 2022.
- [21] O. Awogbemi, I. O. Oluwaleye, and C. A. Komolafe, "A survey of solar energy utilization for sustainable development In Nigeria," *Journal of Multidisciplinary Engineering Science and Technology*, vol. 2, no. 2, pp. 1716–1724, 2015.
- [22] D. A. Neaman, *Semiconductor Physics and Devices Basic Principles*. New York: Raghu Srinivasan, fourth ed., 2012.
- [23] M. C. Scharber and N. S. Sariciftei, "Efficiency of bulk-heterojunction organic solar cells," *Progress in Polymer Science*, vol. 38, no. 12, pp. 1929–1940, 2013.
- [24] S. Izawa, A. Perrot, J.-H. Lee, and M. Hiramoto, "Organic pn homojunction solar cell," *Organic electronics*, vol. 71, pp. 45–49, 2019.
- [25] L. W. McKeen, "Chapter 2 - introduction to the properties of plastic and elastomer films," in *Film Properties of Plastics and Elastomers (Third Edition)* (L. W. McKeen, ed.), *Plastics Design Library*, pp. 19–55, Boston: William Andrew Publishing, third edition ed., 2012.
- [26] *Organic Solar Cells : Materials and Device Physics*. Green Energy and Technology, London: Springer London, elektronisk udgave. ed., 2013.
- [27] N. E. Vollhardt, K. Peter C.; Schore, *Organic Chemistry : Structure and Function*. New York, N.Y: W.H. Freeman and Company, 7. ed. ed., 2014.
- [28] V. K. Ahluwalia, *Green chemistry : environmentally benign reactions*. Cham, Switzerland: Springer, third edition. ed., 2021.
- [29] V. K. Yadav, *Steric and stereoelectronic effects in organic chemistry*. Cham, Switzerland: Springer, 2nd ed. ed., 2021.

- [30] J.-E. Bäckcall, “Palladium-Catalyzed Cross Couplings in Organic Synthesis,” vol. 50005, no. October, pp. 0–12, 2010.
- [31] P. WALLACE and C. TOWNS, “Conjugated polymer preparation via suzuki-coupling in emulsion,” 2011.
- [32] M. G. Melchor, “General Introduction,” in *A Theoretical Study of Pd-Catalyzed C-C Cross-Coupling Reactions*, pp. 1–28, © Springer International Publishing, 2013.
- [33] A. Van Herk and G. R.G, “Emulsion Polymerisation,” in *Chemistry and Technology of Emulsion Polymerisation* (I. John Wiley & Sons, ed.), ch. 1, pp. 46–78, 2013.
- [34] D. Muenmart, A. B. Foster, A. Harvey, M. T. Chen, O. Navarro, V. Promarak, M. C. McCairn, J. M. Behrendt, and M. L. Turner, “Conjugated polymer nanoparticles by Suzuki-Miyaura cross-coupling reactions in an emulsion at room temperature,” *Macromolecules*, vol. 47, no. 19, pp. 6531–6539, 2014.
- [35] C. M. Aitchison, R. S. Sprick, and A. I. Cooper, “Emulsion polymerization derived organic photocatalysts for improved light-driven hydrogen evolution,” *Journal of Materials Chemistry A*, vol. 7, no. 6, pp. 2490–2496, 2019.
- [36] S. Alibert-Fouet, I. Seguy, J.-F. Bobo, P. Destruel, and H. Bock, “Liquid-crystalline and electron-deficient coronene oligocarboxylic esters and imides by twofold benzogenic diels-alder reactions on perylenes,” *Chemistry : a European journal*, vol. 13, no. 6, pp. 1746–1753, 2007.
- [37] C. Methfessel, *Synthesis and Characterization of Amphiphilic Porphyrin-Perylene Dyads: Towards Optoelectronic Membranes in Water*. PhD thesis, 01 2020.
- [38] “Journal of the american chemical society.,” vol. 142, no. 31, 2020.
- [39] J. Kumsampao, C. Chaiwai, P. Chasing, T. Chawanpunyawat, S. Namuangruk, T. Sudyoasuk, and V. Promarak, “A simple and strong electron-deficient 5,6-dicyano[2,1,3]benzothiadiazole-cored donor-acceptor-donor compound for efficient near infrared thermally activated delayed fluorescence,” *Chemistry, an Asian journal*, vol. 15, no. 19, pp. 3029–3036, 2020.
- [40] B. Liu and G. C. Bazan, “Interpolyelectrolyte complexes of conjugated copolymers and dna: Platforms for multicolor biosensors,” *Journal of the American Chemical Society*, vol. 126, no. 7, pp. 1942–1943, 2004.
- [41] R. Wang, C. Zhang, W. Wang, and T. Liu, “Preparation, morphology, and biolabeling of fluorescent nanoparticles based on conjugated polymers by emulsion polymerization,” *Journal of polymer science. Part A, Polymer chemistry*, vol. 48, no. 21, pp. 4867–4874, 2010.
- [42] *Introduction to spectroscopy*. Australia: Cengage Learning, 5. ed. ed., 2015.